Taylor & Francis
Taylor & Francis Group

RESEARCH PAPER

🔓 OPEN ACCESS | Check for updates

Design, synthesis, and evaluation of chalcone-Vitamin E-donepezil hybrids as multi-target-directed ligands for the treatment of Alzheimer's disease

Zhipei Sang[a,b], Qing Song[b], Zhongcheng Cao[b], Yong Deng[b] and Li Zhang[c]

[a]College of Chemistry and Pharmaceutical Engineering, Nanyang Normal University, Nanyang, China; [b]Department of Medicinal Chemistry, West China School of Pharmacy, Sichuan University, Chengdu, China; [c]Department of Elderly Digestive, Sichuan Academy of Medical Sciences, Sichuan Provincial People's Hospital, Chengdu, China

ABSTRACT

A novel series of chalcone-Vitamin E-donepezil hybrids was designed and developed based on multitarget-directed ligands (MTDLs) strategy for treating Alzheimer's disease (AD). The biological results revealed that compound **17f** showed good AChE inhibitory potency (*rat*AChE $IC_{50} = 0.41\,\mu M$; *ee*AChE $IC_{50} = 1.88\,\mu M$). Both the kinetic analysis and docking study revealed that **17f** was a mixed type AChE inhibitor. **17f** was also a good antioxidant (ORAC = 3.3 *eq*), selective metal chelator and *hu*MAO-B inhibitor ($IC_{50} = 8.8\,\mu M$). Moreover, it showed remarkable inhibition of self- and Cu^{2+}-induced $A\beta_{1-42}$ aggregation with a 78.0 and 93.5% percentage rate at $25\,\mu M$, respectively, and disassembled self-induced and Cu^{2+}-induced aggregation of the accumulated $A\beta_{1-42}$ fibrils with 72.3 and 84.5% disaggregation rate, respectively. More importantly, **17f** exhibited a good neuroprotective effect on H_2O_2-induced PC12 cell injury and presented good blood-brain barrier permeability *in vitro*. Thus, **17f** was a promising multi-target-directed ligand for treating AD.

1. Introduction

Alzheimer's disease (AD) is an age-related neurodegenerative disease characterised by deterioration of memory, language, and other cognitive impairments in elder people[1]. Newly available data exhibits that over 50 million dementia patients and the number will be projected to 152 million in 2050[2]. The current therapeutic agents approved by FDA, such as the acetylcholinesterase (AChE) inhibitors (rivastigmine, donepezil, and galantamine) and the *N*-methyl-D-aspartate receptor antagonist (menantine), only present modest symptomatic effects and cannot stop, prevent, or reverse the progression of AD[3,4]. Thus, the development of disease-modifying drugs is a great unmet medical need for AD patients.

Up to now, the exact pathogenesis of AD remains unclear. The amyloid cascade hypothesis states that $A\beta$ aggregates are the triggering event in the pathogenesis of AD[5]. The accumulation of soluble $A\beta$ oligomers leads to the damage and death of neurons and further accelerates the spread of tau-related neurofibrillary tangles, neuroinflammation, and neuronal degeneration and death[6,7]. So, $A\beta$ serves as a major therapeutic target for treating AD. Recently, the failures of current and previous trials of immunotherapy reveal that targeting of $A\beta$ alone might not be enough to prevent or slow AD progression, as multiple mechanisms are involved in AD pathogenesis and their relative contributions might vary at different stages of the disease[8]. The use of appropriate and specific therapeutic targets at different stages of the disease might be a promising way to cure or prevent AD in the future.

Due to the complexity of AD, the success of a therapeutic approach is likely to depend on the simultaneous modulation of more than one AD-relevant target, which leads to a new paradigm in drug discovery for AD, namely the multi-target-directed ligands (MTDLs). MTDLs can hit two or more AD-relevant complementary targets and produce synergistic effects on the disease network by improving clinical outcomes[9–12]. In particular, the MTDLs involving AChE inhibitors have drawn great attention because selective AChE inhibitors could improve cognitive impairment and many promising AChE inhibitor-based multifunctional agents are in progress[13–15].

In addition, the oxidative stress hypothesis states that the generation of excess reactive oxygen species (ROS) is also a major contributor to the progression of AD. The accumulation of ROS leads to the generation of oxidative damage and further damages protein, lipid, and DNA[16]. Moreover, the metal ion hypothesis states that high levels and dysregulation of Cu^{2+}, Fe^{2+}, and Zn^{2+} exist in the brain of AD, which accelerates the aggregation of $A\beta$ and neurotoxic oxidative processes[17,18]. Therefore, antioxidants and biometal chelators offer a promising therapy for the treatment of AD.

Increasing evidences also reveal that high levels of monoamine oxidase-B (MAO-B) are observed in the brain of AD. The excess MAO-B produces hydroxyl radicals, accelerating the former of $A\beta$ plaques[19]. Rasagiline, a selective MAO-B inhibitory drug, has been performed a phase 2 trial in people with mild-to-moderate AD, and it reveals trends to better performance[20].

Chalcones are prominent secondary-metabolite precursors of flavonoids and isoflavonoids in plants. Chalcones possess widely biological activities, particularly, radical-scavenging, anti-inflammatory, MAO-B inhibition, and neuroprotective property contribute to the treatment of AD[21,22]. Many chalcone derivatives have been designed and applied for the development of anti-AD[22–25]. Vitamin E (α-tocopherol) is a fat-soluble antioxidant that can regulate the production of ROS and reactive nitrogen species (RNS) while displaying weak water solubility, and the hydroxy of Vitamin E plays a key role in the antioxidant activity[26]. Donepezil is a commercial AChE inhibitor for the treatment of mild-to-moderate AD, and it has been widely attracted by its AChE inhibitory potency, high selectivity, low toxicity, and good bioavailability. The 1-benzylpiperidine fragment of donepezil is the key pharmacophore of AChE inhibition and indicates good water solubility, and many donepezil hybrids have been developed as MTDLs[13,14,27]. This work plans to create multi-target active small molecules by fusing chalcone, Vitamin E, and donepezil, and then evaluate whether the novel derivatives possess various multifunctional potency and good drug-like properties.

In this work, a series of novel chalcone-Vitamin E-donepezil hybrids were synthesised and developed as multitarget-directed ligands (Figure 1). The evaluation of biological activities includes AChE inhibitory activity, metals chelation property, antioxidant activity, Aβ aggregation inhibition/disaggregation, and MAO-B inhibitory potency.

2. Result and discussion

2.1. Chemistry

In Schemes 1, 2, the synthesis of chalcone-Vitamin E hybrids was described. Firstly, the starting material 1 was reacted with amounts of 1,3-dibromopropane, 1,4-dibromobutane, or 1,6-dibromohexane in anhydrous CH$_3$CN with K$_2$CO$_3$ at 65 °C to get compounds 2a–c. And then, compounds 2a–c were reacted with secondary amines 3a–b[23–25] and diethylamine 3c to afford compounds 4a–b, 5a–c, and 6a–b. Finally, the products 8, 9a–f, and 10 were obtained by the condensation of intermediates 7 with the corresponding benzaldehydes 1, 4a–b, 5a–c, and 6a–b in 50% KOH solution.

For the target compounds 17a–f. Primarily, material 11 was reacted with chloromethyl methyl ether (MOMCl) to give the compound 12, then the key intermediates 13a–b, 14a–b, and 15a–b were synthesised through the condensation of 12 with the corresponding benzaldehydes 1, 4a–b, 5a–b, and 6a–b in alcoholic 50% KOH solution, which was treated with 10% HCl to get the desired products 16 and 17a–f.

2.2. Pharmacology

2.2.1. Ache and BuChE inhibition assay

Ellman's method was employed to assess the AChE and BuChE inhibitory activities of target chalcone-Vitamin E-donepezil hybrids[27,28]. AChE was from cortex homogenate of rat (RatAChE) and electric eel (eeAChE), ratBuChE from rat serum. In the above experiments, donepezil, compounds 8 and 16 were applied as positive compounds. As displayed in Table 1, all the target chalcone-Vitamin E-donepezil hybrids displayed good and high selective AChE inhibitory activity. Compounds 9d and 17f demonstrated the best AChE inhibitory potency in the two skeleton series, respectively, with their IC$_{50}$ values of 0.32 and 0.41 μM, respectively.

In the preliminary experiments, as expected, compounds 8 (IC$_{50} > 500$ μM) and 16 (IC$_{50} > 500$ μM) exhibited no significant inhibition of AChE. Based on our previous work, the 2-methoxybenzyl groups were in favour of improving AChE inhibitory activity, thus the 2-methoxybenzyl substituent groups were introduced into the parent compounds 8 and 16 to obtain compounds 9a–f and 17a–f, respectively, dramatically showing significant AChE inhibitory activities (IC$_{50}$ was 3.45–0.32 μM). In particular, the compounds 9d and 17f exhibited good inhibitory potency with their IC$_{50}$ values of 0.32 and 0.41 μM, respectively. Moreover, the compounds (9b, 9d, 9f, 17b, 17d, and 17f) possessing the N-ethyl
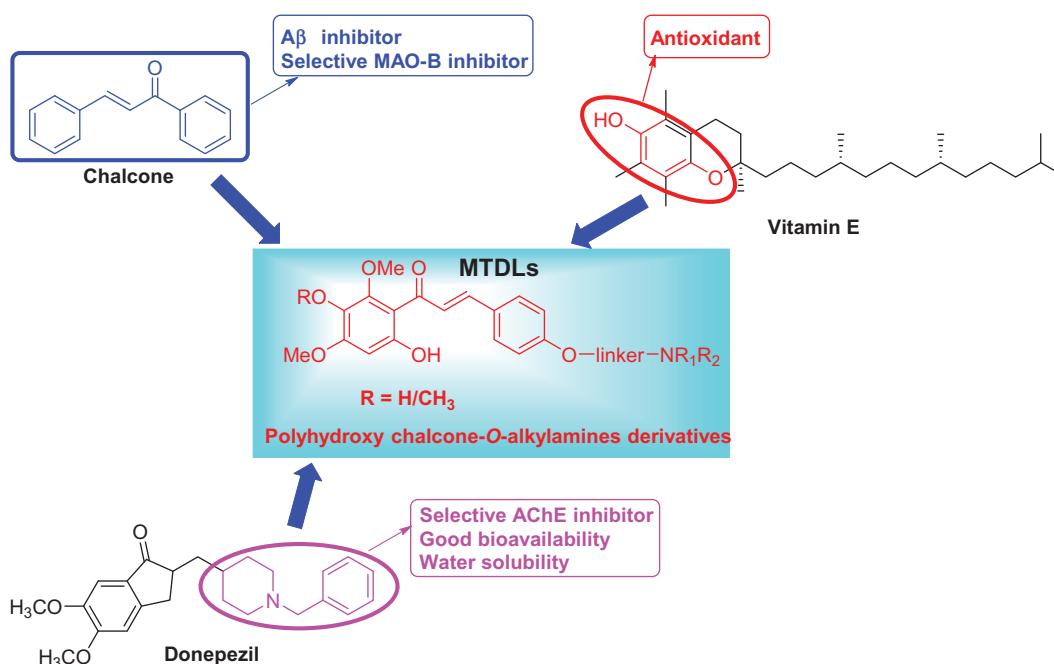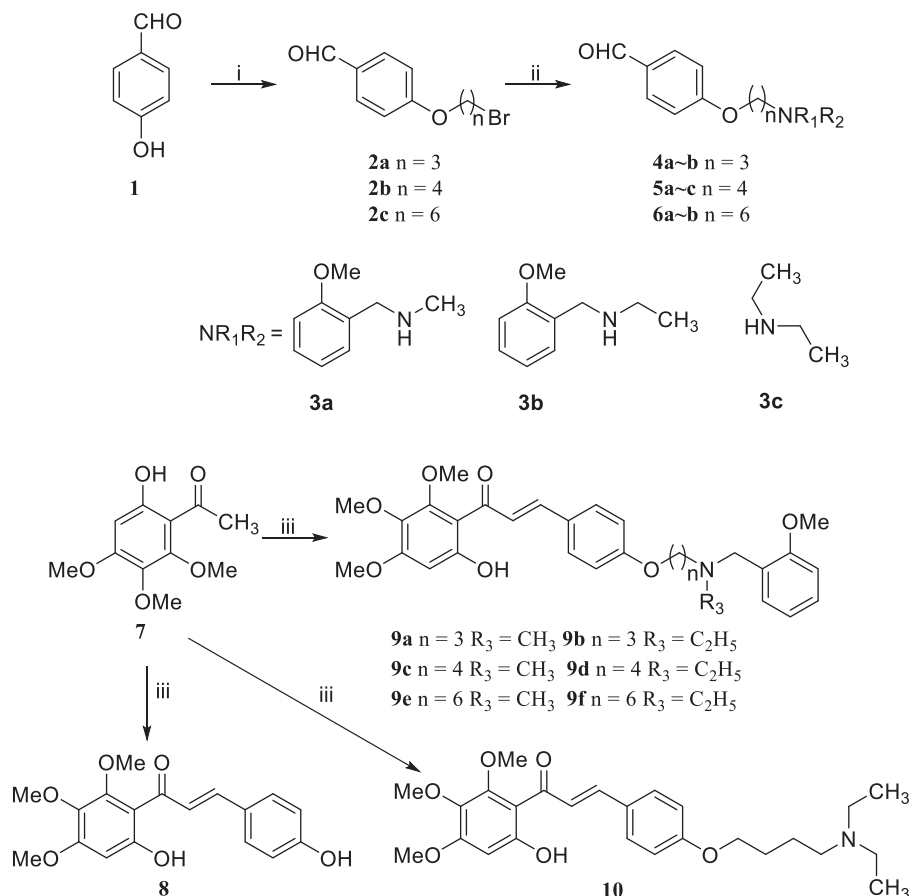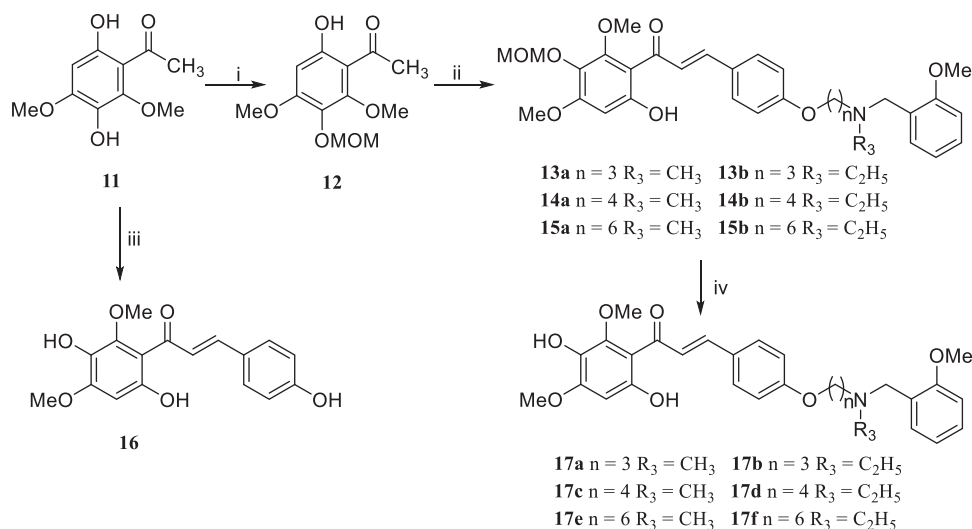

Figure 1. Design strategy for chalcone-Vitamin E-donepezil hybrids.

Scheme 1. Synthesis of target chalcone-Vitamin E-donepezil hybrids **8**, **9a–f**, and **10**. Reaction conditions: (i) Br(CH$_2$)$_n$Br, K$_2$CO$_3$, CH$_3$CN, 65 °C, 6–10 h; (ii) NHR$_1$R$_2$ (**3a–c**), K$_2$CO$_3$, CH$_3$CN, refluxed, 6–8 h; (iii) **1**, **4a–b**, **5a–c**, and **6a–b**, 50% KOH, r.t., 3–4 days.

Scheme 2. Synthesis of target chalcone-Vitamin E-donepezil hybrids **16** and **17a–f**. Reagents and conditions: (i) chloromethyl methyl ether, (i-Pr)$_2$EtN, acetone, 50 °C, 6–8 h; (ii) **4a–b**, **5a–b**, and **6a–b**, 50% KOH, r.t., 3–4 days; (iii) **1**, 50% KOH, r.t., 3–4 days; (iv) 10% HCl, room temperature, overnight.

group on the terminal nitrogen showed better inhibition potency than the corresponding compounds (**9a**, **9c**, **9e**, **17a**, **17c**, and **17e**) with *N*-methyl group, which was supported by our previous work[24]. In addition, to study the importance of benzylamines groups, we replaced the *N*-ethyl-2-methoxy-benzenemethanamine group of compound **9d** with diethylene group to furnish compound **10** (IC$_{50}$ = 4.94 μM), giving a dropped obviously AChE

inhibitory potency. These results indicated that the electron density of the aromatic ring, especially the *N*-ethyl-2-methoxy-benzenemethanamine group, contributed to the AChE inhibitory activity. Furthermore, compared with our previous work of chalcone derivatives, when introducing dual *O*-alkylamines into the chalcone skeleton, the AChE inhibitory activity was obviously enhanced[24]. When the *O*-alkylamines fragment was replaced at 3 positions, the

chalcone derivatives showed significant selective BuChE inhibitory activity[23].

For BuChE inhibition assay, all chalcone-Vitamin E-donepezil hybrids proved to be inactive or weak active on ratBuChE. Based on the above results, compounds **9d** and **17f** were selected for metal chelation abilities.

2.2.2. Antioxidant activity

The Oxygen Radicals Absorbance Capacity by Fluorescence (ORAC-FL) method was employed to evaluate antioxidant activities of the synthesised target compounds with Trolox as a reference compound[29,30]. As shown in Table 1, the positive compound Vitamin E showed good antioxidant activity with an ORAC-FL value of 2.6

eq, all the target chalcone-Vitamin E-donepezil hybrids demonstrated good antioxidant potency with ORAC-FL values ranging from 0.90 to 3.4 eq, but displayed lower potency than the parent compounds **8** (5.4 eq) and **16** (7.8 eq). Among these compounds, compounds **17a–f** (ORAC-FL values of 2.6–3.4 eq) with two hydroxyl groups exhibited more potent antioxidant activity than other analogues **9a–f** and **10** (ORAC-FL values of 0.93–1.04 eq) with one hydroxyl group. The data revealed that the number of free hydroxyls contributed to the antioxidant potency. Compounds **9d** and **17f** showed significant antioxidant potency with ORAC-FL values of 0.96 and 3.3 eq, respectively. According to the above data, compound **17f** was chosen for kinetic characterisation study and molecular modelling study.

2.2.3. Kinetic characterisation of AChE inhibition

To explore the possible mechanism for chalcone-Vitamin E-donepezil hybrids on AChE. The significant compound **17f**, with good AChE inhibitory activity and antioxidant activity, was selected to investigate the inhibition mechanism of AChE[27,28]. The reciprocal Lineweaver-Burk plots analysis (Figure 2) suggested that both increasing slopes (decreased V_{max}) and intercepts (higher K_m) at increasing concentration of **17f**. The intersection point fell in the second quadrant, revealing a mixed-type inhibition.

2.2.4. Molecular docking of 17f with AChE

The possible interacting mechanism of **17f** with AChE (PDB code: *1EVE*) was performed using AUTODOCK 4.2 package[25]. As displayed in Figure 3, the *O* atom of the methoxyl group interacted with important residues Phe288 and Arg289, respectively. The H atom of one of the hydroxyl groups presented one intermolecular hydrogen bonding with Arg289. The H atom of another hydroxyl group presented one intermolecular hydrogen bonding with residue Tyr334. In addition, the carbonyl group displayed one intermolecular hydrogen bonding with residue Phe288. Moreover, the N atom of *N*-(2-methoxybenzyl)ethanamine fragment interacted with important residue Ser122 via one intermolecular hydrogen bonding. Furthermore, the benzene ring of compound **17f** formed one π–π interaction with residue Phe330. Besides, some hydrophobic interactions were presented between compound **17f** and

Table 1. AChE and BuChE inhibitory potency and oxygen radical absorbance capacity (ORAC, Trolox equivalent) by chalcone-Vitamin E-donepezil hybrids, Vitamin E, and donepezil.

Compds.	IC_{50} (μM) ± SD[a]			SI[e]	$ORAC$[f]
	Rat AChE[b]	*Ee*AChE[c]	*Rat*BuChE[d]		
8	>500	>500	>500	–	5.4 ± 0.01
16	>500	>500	>500	–	7.8 ± 0.01
9a	3.12 ± 0.02	1.46 ± 0.02	>500	>160.3	1.01 ± 0.01
9b	0.67 ± 0.01	1.62 ± 0.01	>500	>746.3	0.93 ± 0.01
9c	1.77 ± 0.01	1.50 ± 0.02	>500	>282.5	0.97 ± 0.01
9d	0.32 ± 0.02	1.20 ± 0.01	451 ± 1.68	1409.4	1.01 ± 0.2
9e	1.68 ± 0.01	1.00 ± 0.03	>500	>297.6	0.99 ± 0.02
9f	0.61 ± 0.01	1.78 ± 0.02	>500	>819.7	0.96 ± 0.01
10	4.94 ± 0.02	2.72 ± 0.02	>500	>101.2	1.02 ± 0.01
17a	3.45 ± 0.03	2.30 ± 0.01	326 ± 10.7	94.5	3.1 ± 0.02
17b	0.73 ± 0.01	3.16 ± 0.02	155 ± 5.8	212.3	2.9 ± 0.02
17c	1.63 ± 0.02	3.74 ± 0.03	>500	>306.7	2.8 ± 0.01
17d	0.58 ± 0.01	3.68 ± 0.02	406 ± 15.2	700	3.1 ± 0.01
17e	1.40 ± 0.02	2.16 ± 0.01	>500	>357.1	3.4 ± 0.02
17f	0.41 ± 0.02	1.88 ± 0.01	>500	>1219.5	3.3 ± 0.01
Donepezil	0.015 ± 0.002	0.12 ± 0.01	20.7 ± 1.36	1380	n.t.[g]
Vitamin E	–	–	–	–	2.6 ± 0.06

[a]IC_{50} values were expressed as ±SD μM by three independent experiments.
[b]*rat*AChE was from cortex homogenate of rat.
[c]*ee*AChE was from electric eel AChE.
[d]*rat*BuChE was from serum of rat.
[e]SI = Selectivity index = IC_{50} (BuChE)/IC_{50} (AChE).
[f]The ORAC values are expressed as μM of Trolox equivalent/μM of compounds.
[g]n.t. = no test.

Figure 2. Steady-state inhibition by **17f** of AChE hydrolysis of acetylthiocholine (ATCh).
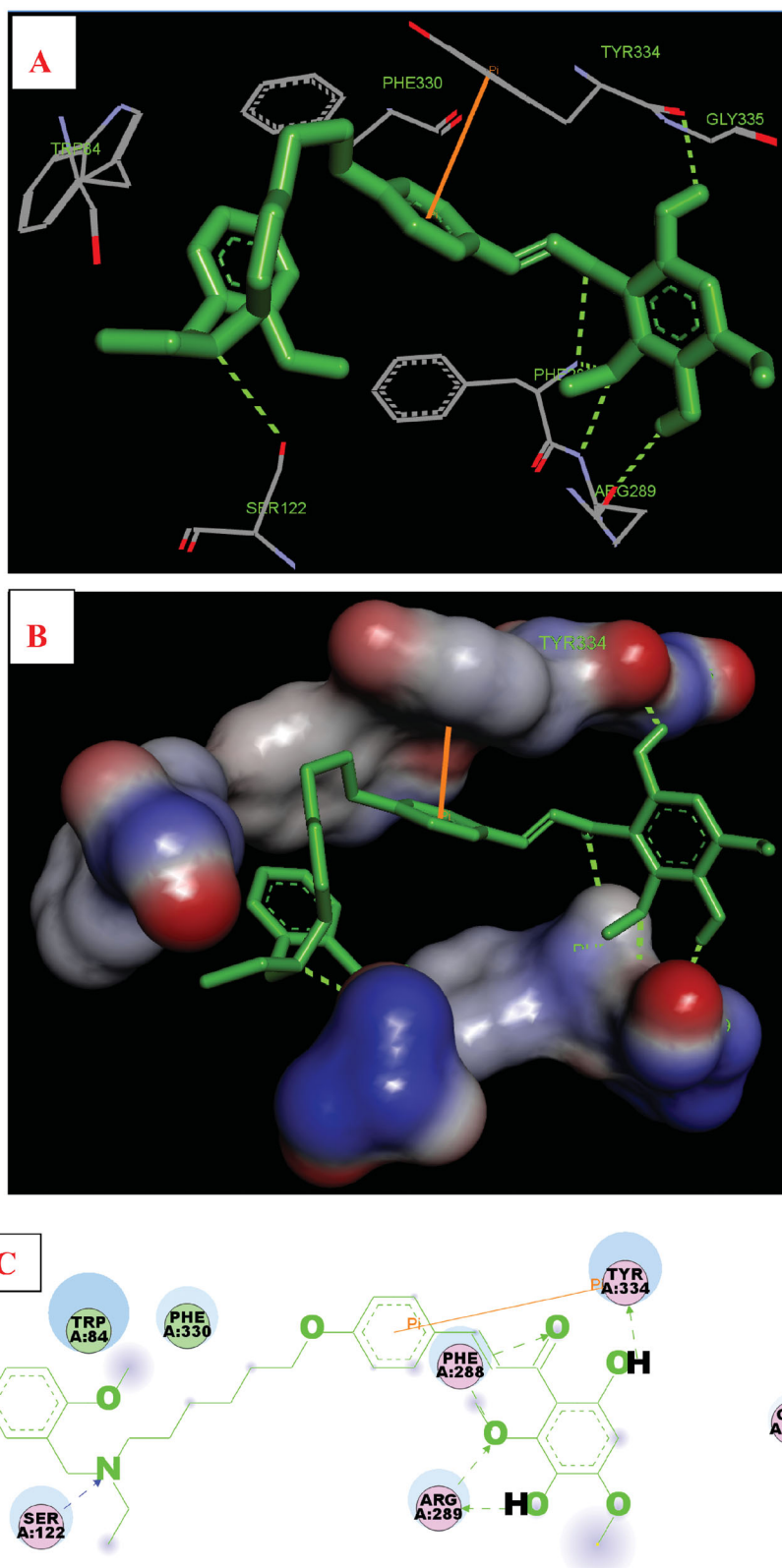
Figure 3. Compound 17f (green stick) interacted with AChE (PDB code: 1eve) (A) Interactions in the active site. (B) 3D docking model. (C) 2D docking model.

residues (such as Trp84, Ser122, Arg289, Phe288, Tyr334, Gly335, and Phe330). The result also revealed that 17f occupied the catalytic site, the mid-gorge site, and the peripheral site, offering a possible mechanism for the high AChE inhibitory activity.

2.2.5. Molecular dynamics (MD) simulations

The stability of docked binding pose of the compound 17f-AChE complex was analysed by molecular dynamics simulation analysis using Amber 16[31]. Figure 4(A) displayed that the root means

Figure 4. (A) RMSD analysis of compound 17f (green stick) in AChE (PDB code: 1eve). (B) The docking model for 17f into the protein crystal structure of AChE (PDB code: 1eve).

square deviations (RMSD) analysis of compound 17f with the amino acid residues of AChE. The results indicated that the RMSDs of all the replicas for the six simulated systems show relatively stable fluctuations after 50 ns of the MSMD simulations, suggesting that the six simulated systems basically reach equilibrium. Figure 4(B) showed the key residues and interactions modes of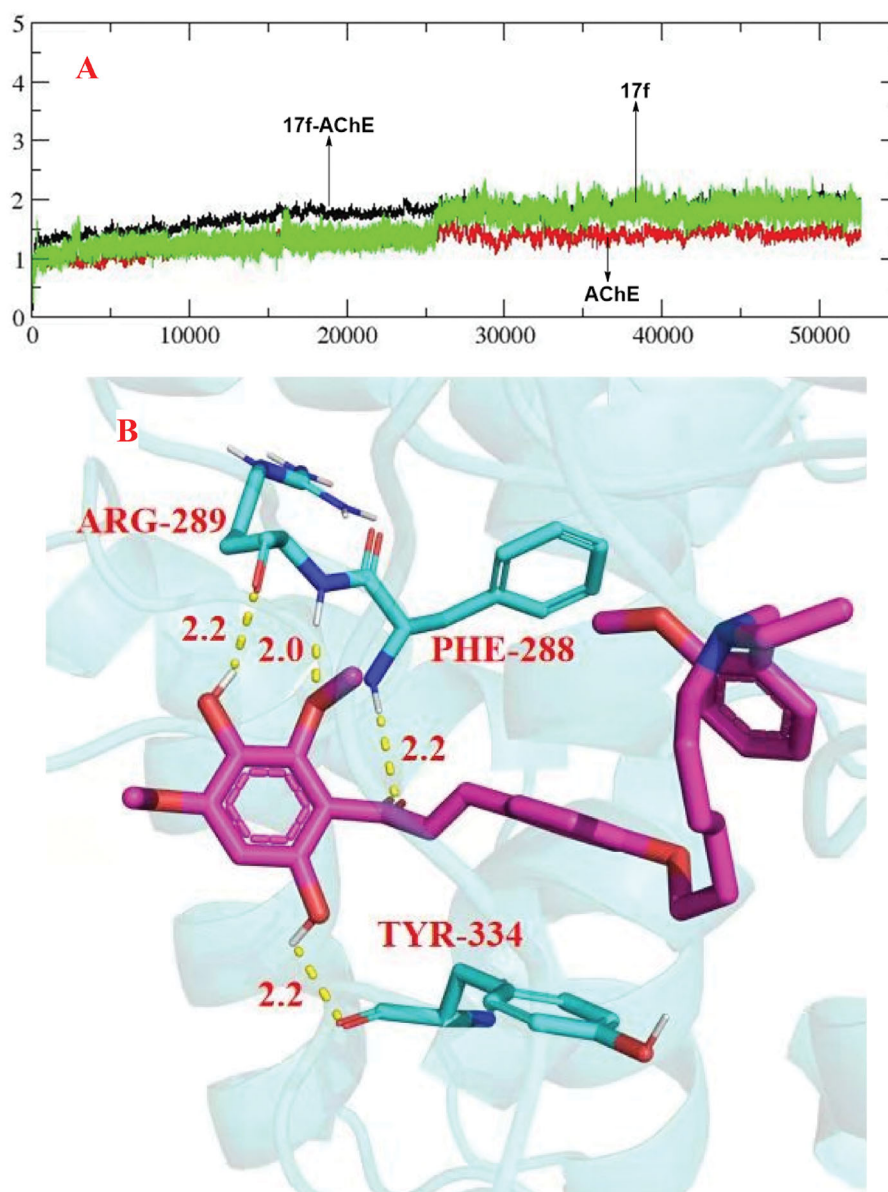 17f with AChE, and four intermolecular hydrogen bonding were observed. The two hydroxy groups of 17f formed one intermolecular hydrogen bonding with the Arg289 (2.2 Å) and Tyr334 (2.2 Å) residues, respectively. The oxygen atom of the methoxy group formed a key intermolecular hydrogen bonding with the Arg289 (2.0 Å) and the oxygen atom of the carbonyl group interacted with key residue Phe288 via one intermolecular hydrogen bonding.

2.2.6. Propidium iodide displacement assay

Given the results from the kinetic study, molecular docking and dynamic simulations, compound 17f has significant interactions with PAS residues of AChE. Therefore, the affinity of compound 17f at 10 and 50 μM concentrations for the PAS-binding was tested by propidium iodide displacement assay[32–34]. As listed in Table 2, the binding of compound 17f to PAS displaced

Table 2. The results of propidium iodide displacement assay and inhibition of huAChE-induced Aβ aggregation towards compound 17f and donepezil.

Compound	Propidium iodide displacement from AChE PAS (% inhibition)[a]		% Inhibition of huAChE-induced Aβ aggregation[b]
	10 μM	50 μM	
17f	23.9 ± 1.6	34.2 ± 2.3	53.9 ± 3.7
Donepezil	20.4 ± 1.3	32.7 ± 2.6	24.3 ± 2.1

[a]Propidium iodide displacement assay was performed on AChE to test the ability of compounds to displace propidium with reference to the donepezil at 10 and 50 μM. Data are presented as the mean ± SEM of three independent experiments.
[b]Inhibition of human AChE-induced $A\beta_{1-40}$ aggregation was tested using ThT assay, the concentration of tested compounds and $A\beta_{1-40}$ was 100 and 230 μM, respectively, and the $A\beta_{1-40}/Hu$AChE ratio was equal to 100/1. Data are presented as the mean ± SEM of three independent experiments.

propidium iodide and resulted in decreased fluorescence intensity. Compared with donepezil (10 μM = 20.4%, 50 μM = 32.7%), compound **17f** displayed slightly higher displacement of propidium iodide (10 μM = 23.9%, 50 μM = 34.2%), which was in agreement with computational studies.

2.2.7. Effects on self-mediated Aβ$_{1-42}$ aggregation

To determine the effects of the chalcone-Vitamin E-donepezil hybrids on self-induced Aβ$_{1-42}$ aggregation, the inhibition assay and disaggregation assay were performed using the thioflavin T (ThT) fluorescence assay[29]. Curcumin compounds **8** and **16** were also tested. The data were collected in Table 3. For the inhibition assay, the precursor compounds **8** (23.1%) and **16** (27.7%) indicated lower inhibitory activity than curcumin (47.3%), and donepezil exhibited no significant inhibition potency (under 5% inhibition ratio at 25 μM). The target compounds (**9a–f**, **10**, and **17a–f**) showed exhibited more inhibitory potency than curcumin.

Generally, compounds **17a–f** indicated better inhibitory activity than other compounds. Seen from the screen data, replacing the N-ethyl-2-methoxy-benzenemethanamine group of **9b** (63.4%) with the diethylene group to obtain the compound **10**, getting a waned dramatically inhibition ratio of 37.7%. Compound **17f** showed higher inhibition potency with an inhibition ratio of 78.0%. These results demonstrated that the hydroxyl group at the 2- and 4-position in the acetophenone moiety (A ring) could play an important role in inhibiting self-mediated Aβ$_{1-42}$ aggregation, and the 2-methoxybenzyl substitutions contributed to the inhibition potency, however, the diethylamine group might be the disadvantageous effect on inhibitory potency.

For disaggregation assay. The data in Table 3 displayed that target compounds exhibited different disaggregation abilities, inhibition ratio ranging from 22.2 to 75.9%. Compound **17f** exhibited remarkably disaggregation potency (72.3%).

Further, transmission electron microscopy (TEM) was employed to observe the degree of Aβ$_{1-42}$ aggregation. As presented in

Table 3. Inhibition and disaggregation potency of Aβ$_{1-42}$ aggregation by donepezil, curcumin, and chalcone-Vitamin E-donepezil hybrids.

Compds.	Inhibition of Aβ$_{1-42}$ aggregation (%)[a]		Disaggregation of Aβ$_{1-42}$ aggregation (%)[a]	
	Self-induced[b]	Cu^{2+}-induced[c]	Self-induced[d]	Cu^{2+}-induced[e]
8	23.1 ± 0.01	33.2 ± 0.01	n.t.[f]	n.t.[f]
16	27.7 ± 0.02	38.1 ± 0.01	n.t.[f]	n.t.[f]
9a	57.4 ± 0.01	66.2 ± 0.02	26.8 ± 0.02	54.2 ± 0.02
9b	63.4 ± 0.03	71.6 ± 0.01	22.2 ± 0.03	55.1 ± 0.22
9c	65.0 ± 0.01	74.1 ± 0.02	45.7 ± 0.12	66.6 ± 0.36
9d	72.7 ± 0.02	72.4 ± 0.01	33.0 ± 0.08	63.2 ± 0.63
9e	65.3 ± 0.02	76.2 ± 0.04	58.2 ± 0.01	77.0 ± 0.57
9f	69.0 ± 0.01	75.0 ± 0.02	62.8 ± 0.03	81.4 ± 0.68
10	37.7 ± 0.02	49.4 ± 0.02	25.6 ± 0.03	26.2 ± 0.28
17a	67.4 ± 0.04	91.1 ± 0.01	29.9 ± 0.03	84.6 ± 0.03
17b	82.1 ± 0.01	90.2 ± 0.02	60.2 ± 0.03	82.8 ± 0.03
17c	68.4 ± 0.02	92.5 ± 0.03	75.9 ± 0.03	79.1 ± 0.15
17d	73.8 ± 0.01	91.7 ± 0.02	45.7 ± 0.16	79.8 ± 0.03
17e	65.7 ± 0.03	96.2 ± 0.02	74.8 ± 0.31	83.7 ± 0.03
17f	78.0 ± 0.02	93.5 ± 0.01	72.3 ± 0.06	84.5 ± 0.35
Donepezil	n.a.[g]	n.t.[f]	n.t.[f]	n.t.[f]
Curcumin[h]	47.3 ± 0.01	76.5 ± 0.02	n.t.[f]	56.5 ± 0.21

[a]Inhibition and disaggregation experiments of Aβ$_{1-42}$ aggregation using ThT assay. The experiments were performed three times and the results were expressed as ±SD.
[b]Inhibition potency of self-mediated Aβ$_{1-42}$ aggregation at 25 μM.
[c]Inhibition potency of Cu^{2+}-mediated Aβ$_{1-42}$ aggregation at 25 μM.
[d]Disaggregation potency of self-mediated Aβ$_{1-42}$ aggregation at 25 μM.
[e]Disaggregation potency of Cu^{2+}-mediated Aβ$_{1-42}$ aggregation at 25 μM.
[f]n.t. = not tested.
[g]n.a. = no active, meaning inhibition rate was <5.0% at 25 μM.
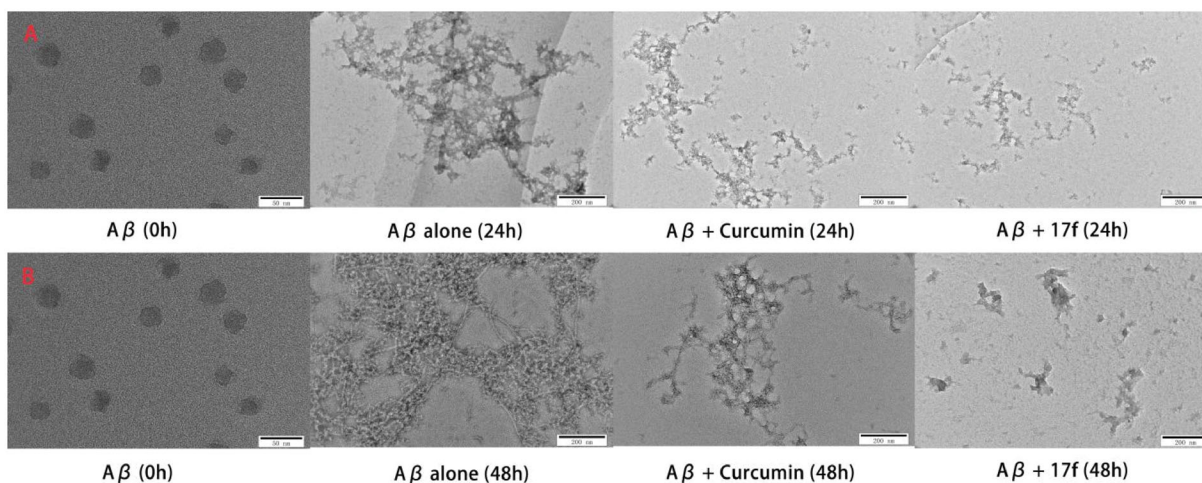[h]The concentration of Curcumin was 25 μM.

Figure 5. TEM images analysis of self-medicated Aβ$_{1-42}$ aggregation by curcumin and compound **17f**. (A) Inhibition experiments. (B) Disaggregation experiments.

Figure 5(A), the fresh $A\beta_{1-42}$ aggregated into amyloid fibrils after 24 h incubation, when treating with curcumin and compound **17f**, respectively, only small $A\beta$ aggregates were observed, which supported the ThT binding assay results. A similar phenomenon was also observed in disaggregation self-induced $A\beta_{1-42}$ aggregation experiments (Figure 5(B)). Therefore, both the ThT assay and TEM images suggested **17f** produced significant inhibition and disaggregation effect on self-mediated $A\beta_{1-42}$ aggregation.

2.2.8. Effects on huAChE-induced $A\beta_{1-40}$ aggregation by 17f

Accumulated evidence showed that the PAS of AChE could bind to the $A\beta$ and accelerated the formation of amyloid fibrils. Compound **17f** was chosen to perform the inhibition experiment of hAChE-induced $A\beta_{1-40}$[30]. As indicated in Table 2, **17f** significantly inhibited huAChE-induced $A\beta_{1-40}$ aggregation with a 53.9% inhibition rate, which was better than that of donepezil (24.3%).

2.2.9. Metal chelation properties

The representative AChE inhibitors **9d** and **17f** were selected to assess the chelation properties using Cu^{2+}, Zn^{2+}, Al^{3+}, and Fe^{2+} by UV-vis spectrometry[29,30]. As displayed in Figure 6, after $CuCl_2$ and $AlCl_3$ were added to a solution of **9d**, the characteristic peak produced a red shift from 362 to 444 and 376 nm, respectively, revealing the formation of **9d**-Cu^{2+} and **9d**-Al^{3+} complex. Correspondingly, the characteristic peak presented no obvious shift when $FeSO_4$ and $ZnCl_2$ were added. For compound **17f**, the characteristic peak generated a red shift from 350 to 422 and 370 nm after adding $CuCl_2$ and $AlCl_3$, respectively, however, there was no significant shift when $FeSO_4$ and $ZnCl_2$ were added. This phenomenon suggested that the compounds **9d** and **17f** were selective chelating agents.

In addition, the molar ratio method was employed to evaluate the stoichiometry of the **17f**-Cu^{2+} complex through preparing the solution of **17f** with increasing $CuCl_2$ at 422 nm. As displayed in Figure 7, the absorbance linearly increased at first and then tended to be stable. The two straight lines intersected at a mole fraction of 1.03, revealing a 1:1 stoichiometry for complex **17f**-Cu^{2+}. A similar method was carried out, for compound **9d** with $CuCl_2$ revealed a break at 1.1 and 1.06, revealing a 1:1 stoichiometry for the **9d**-Cu^{2+} complex.

2.2.10. Effects on Cu^{2+}-mediated $A\beta_{1-42}$ aggregation and disaggregation

Similarly, the inhibition assay and disaggregation assay were employed for the Cu^{2+}-mediated $A\beta_{1-42}$ aggregation to assess the ability of chalcone-Vitamin E-donepezil hybrids using ThT binding assay[29,30]. For inhibition potency. As shown in Table 3, the precursor compounds **8** (33.2%) and **16** (38.1%) exhibited low inhibition potency, target compounds exhibited moderate-to-good inhibition potencies compared with curcumin (76.5%). Compound **17f** demonstrated remarkable inhibition potency (93.5%). In general, the compounds **17a–f** with two hydroxyl groups displayed better inhibitory activity than the other target compounds. In addition, replacing the N-ethyl-2-methoxy-benzenemethanamine group of **9b** (71.6%) with the diethylene group to get compound **10** (49.4%) with the lowest inhibitory activity. These results implied that the hydroxyl groups acted as a key role in the inhibition of Cu^{2+}-mediated $A\beta_{1-42}$ aggregation, the 2-methoxybenzyl groups substitutions contributed to the inhibition potency, the aliphatic amine (such as diethylamine) provided an adverse influence on inhibition potency.

For disaggregation potency, most target compounds exhibited significant disaggregation potency. Among them, compound **10**
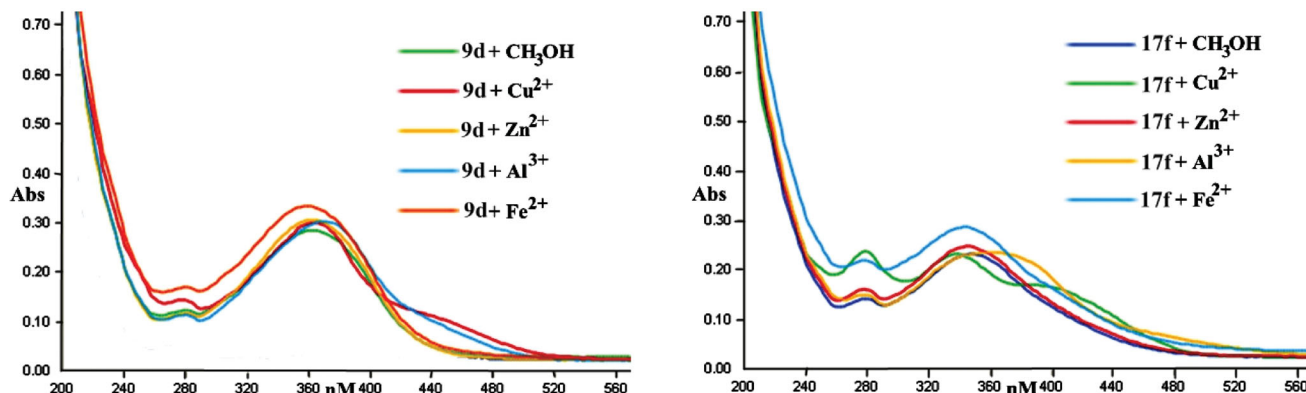

Figure 6. The UV spectrum of compounds **9d** and **17f** alone or in the presence of $CuCl_2$, $AlCl_3$, $ZnCl_2$, and $FeSO_4$. The final concentration was 37.5 μM.
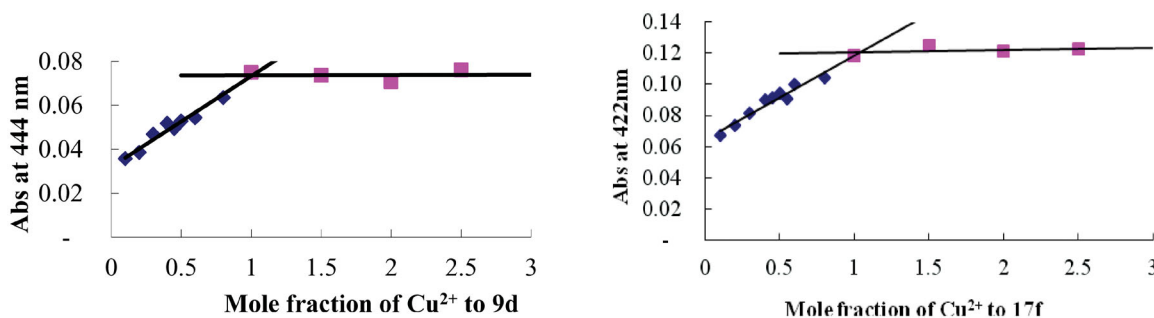

Figure 7. Determination of the stoichiometry of complex compound-Cu^{2+} by using the molar ratio method. The final concentration of compounds **9d** and **17f** was 37.5 μM, with ascending amounts of $CuCl_2$.
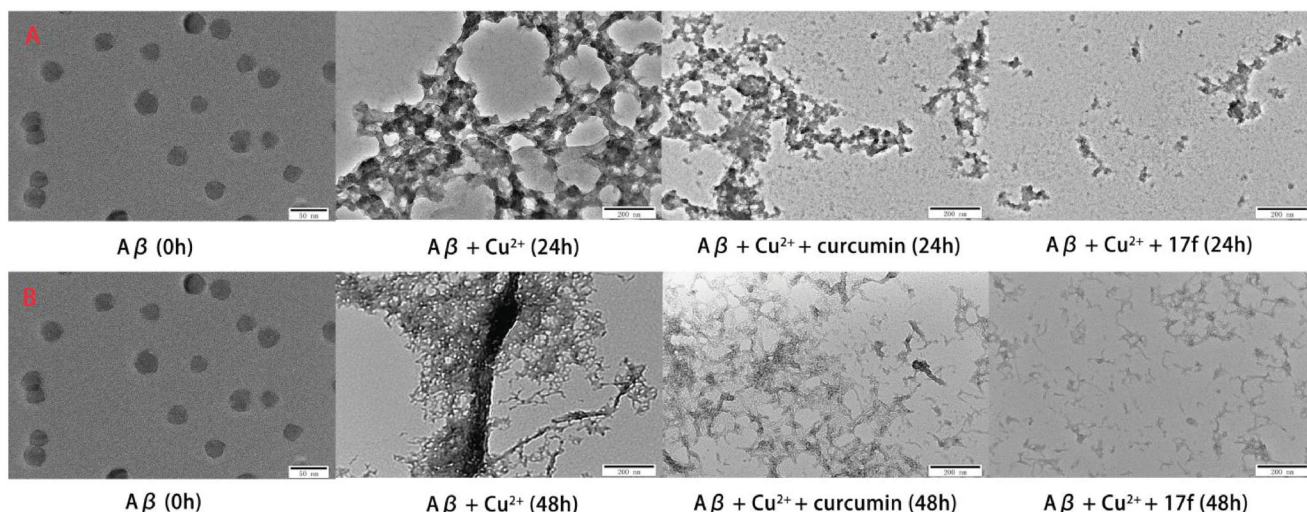
Figure 8. TEM images analysis of Cu^{2+}-mediated $A\beta_{1-42}$ aggregation by curcumin and compound **17f**. (A) Inhibition experiments. (B) Disaggregation experiments.

(26.2%) showed the lowest disaggregation ability and it might be that the diethylene group produced disadvantageous effects on disaggregating potency. Compound **17f** indicated significant disaggregation potency with a disaggregation ratio of 84.5% and it showed that **17f** disaggregated Cu^{2+}-mediated $A\beta_{1-42}$ fibrils. In short, compound **17f** can inhibit and disaggregate Cu^{2+}-mediated $A\beta_{1-42}$ fibrils, which were also supported by the TEM images in Figure 8.

2.2.11. Molecular docking of 17f with Aβ

Molecular docking was employed to investigate the binding mechanism of **17f** with $A\beta_{1-42}$ (PDB: 1BA4). As displayed in Figure 9, compound **17f** was located at the C-terminus hydrophobic area of $A\beta$. The oxygen atom of the hydroxyl group presented one intermolecular hydrogen bonding with ASP1, the methoxy group of *N*-(2-methoxybenzyl)ethanamine fragment formed one intermolecular hydrogen bonding with Asn27, and the benzene ring of *N*-(2-methoxybenzyl)ethanamine fragment interacted with Asp 1 via one δ–π interaction. Besides, compound **17f** presented some hydrophobic interactions with the amino acid residues LYS16, ASP1, Phe19, PHE20, Glu22, Asp23, and ASN27. These observed interactions might provide a rational mechanism for the binding of $A\beta_{1-42}$ with **17f**.

2.2.12. Inhibitory potency of huMAO-a and huMAO-B

The fluorescence method was employed to evaluate the inhibitory activity of huMAO-A and huMAO-B (recombinant human enzyme) by target chalcone-Vitamin E-donepezil hybrids[26]. The data from Table 4 showed that most of the target derivatives were significantly selective huMAO-B inhibitors, except compounds **17a**, **17b**, and **17c**. Among these compounds, compound **9e** (IC$_{50}$ = 2.5 µM) displayed the best MAO-B inhibitory potency, and the selectivity index value was 15.1. In general, compounds **17a–f** with two hydroxyl groups exhibited slightly weaker inhibitory activity than compounds **9a–f** with one hydroxyl group. Compound **17f** presented selective MAO-B inhibitory activity (IC$_{50}$ = 8.8 µM; SI = 4.3).

2.2.13. Molecular modelling of 17f with MAO-B

Compound **17f** was selected to perform the docking with human MAO-B (PDB code: 2V60)[23]. As indicated in Figure 10, the O atom

of methoxyl group in compound **17f** interacted with key residues Leu345 and Ala325Thr 201 via one intermolecular hydrogen bonding, respectively. The O atom of the hydroxyl group in **17f** interacted with residue Ala325 via one intermolecular hydrogen bonding. Moreover, the carbonyl group interacted with residues Ala325 and Tyr326 via one intermolecular hydrogen bonding, respectively. Furthermore, the N atom of *N*-(2-methoxybenzyl)ethanamine moiety interacted with Tyr326 and Thr201 via one intermolecular hydrogen bonding, respectively. In addition, there were some hydrophobic interactions could be found between compound **17f** and residues (such as Leu345, Tyr60, Thr201, Glu84, Tyr326, and Ala325). Therefore, the observed interactions offered a rational mechanism for the high MAO-B inhibitory potency towards **17f**.

2.2.14. Neuroprotective effects

Firstly, the cytotoxicity of compound **17f** was tested using an MTT assay. As shown in Figure 11(A), compound **17f** did not show obvious cytotoxicity until the concentration increased up to 50 µM, showing a wide safety range. Subsequently, the neuroprotective effects of **17f** against H_2O_2–induced PC12 cell injury were investigated through MTT assay and lactate dehydrogenase (LDH) assay, and Vitamin E (VE) acted as the positive drug[29,30]. As shown in Figure 11(B), PC12 cells were cultured and exposed to 100 µM H_2O_2 for 1 h to establish the oxidative damage model and the cell viability fleetly declined to 47.1% ($p < 0.01$) compared with the normal group. When the PC12 cells were treated with 100 µM Vitamin E (VE), the cell viability increased to 68.2% ($p < 0.01$). Subsequently, the PC12 cells were treated with 10 and 50 µM compound **17f**, respectively. The cell viability added up to 65.7% ($p < 0.05$) and 73.4% ($p < 0.05$), respectively, indicating a better neuroprotective effect than VE. Further, the experiment was also investigated by LDH assay. As shown in Figure 11(C), the LDH vitality suddenly enhanced to 712.7 ($p < 0.01$) compared with the vehicle group (602.3) after PC12 cells were exposed to 100 µM H_2O_2. When PC12 cells were treated with 100 µM VE, the LDH vitality was 654.7 ($p < 0.01$). Subsequently, when PC12 cells were treated with 10 and 50 µM compound **17f**, respectively, the LDH vitality declined to 621.3 ($p < 0.01$) and 549.7 ($p < 0.05$), respectively. In short, the above results exhibited that compound **17f**
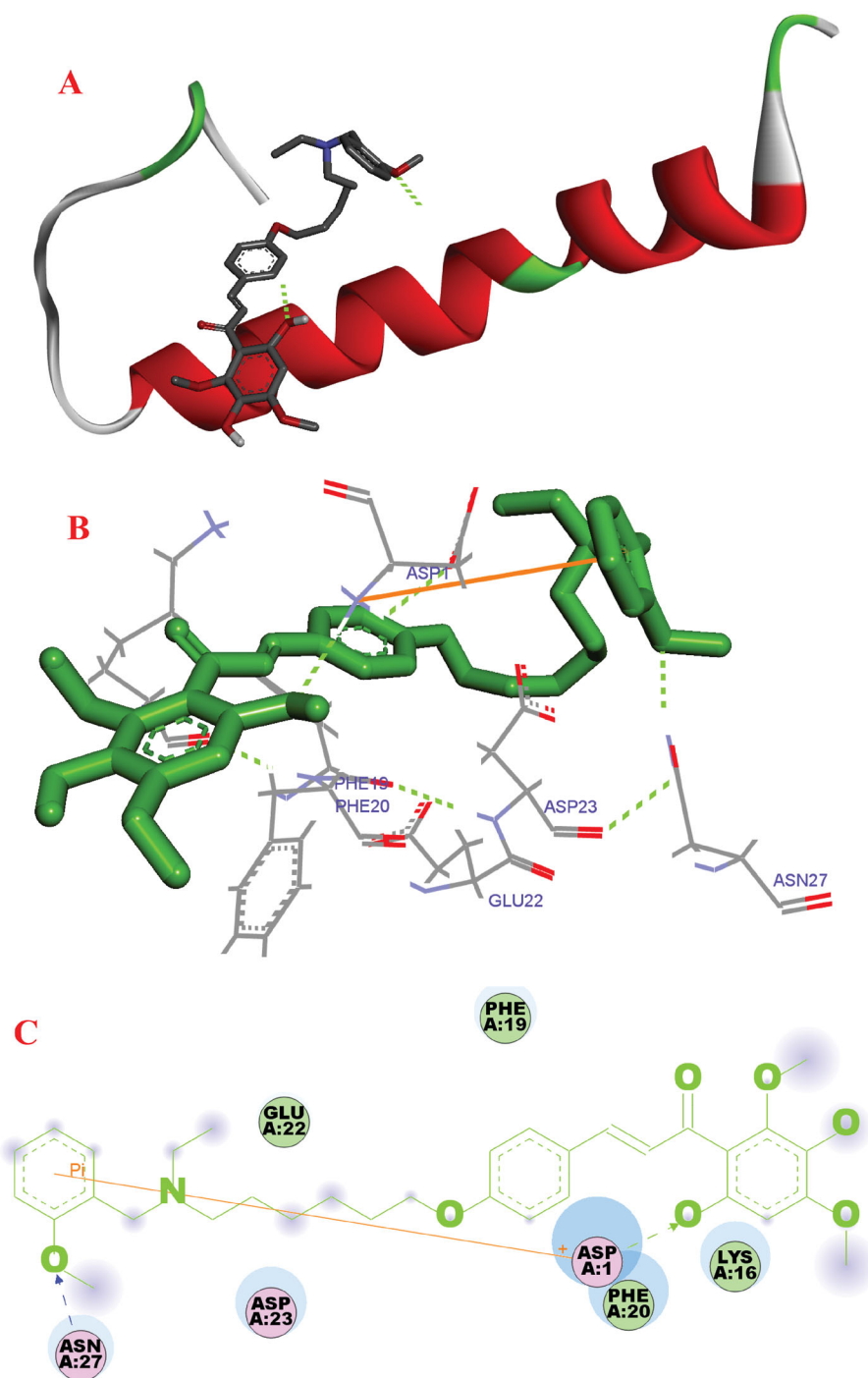
Figure 9. Docking studies of **17f** with $A\beta_{1-42}$ (PDB ID: 1BA4). (A) Cartoon model. (B) Interactions in the C-terminus of the active site. (C) 2D docking model.

exhibited a good neuroprotective effect against H_2O_2-induced PC12 cell injury by MTT and LDH assay.

2.2.15. Blood–brain barrier assay in vitro

The parallel artificial membrane permeation assay of the blood–brain barrier (PAMPA-BBB) was employed to investigate BBB permeability of **17f**[35,36]. Eleven commercial drugs were chosen and the permeability was compared with reported data to validate this method and produced a good linear correlation, $P_e(\text{exp}) = 0.9163P_e(\text{bibl.}) - 0.2247$ ($R^2 = 0.9558$). Based on this equation and the limit established, we concluded that derivatives with permeability P_e ($\times 10^{-6}$ cm/s) $> 3.44 \times 10^{-6}$ cm/s possess high BBB permeation; $3.44 > P_e > 1.61$ displayed uncertain BBB permeation; $P_e < 1.61$ showed low BBB permeation. The measured data in Table 5 revealed that the positive compounds verapamil and diazepam could cross the BBB, while enoxacin could not cross the BBB. The data also displayed **17f** could cross the BBB.

3. Conclusions

In conclusion, a novel series of chalcone-Vitamin E-donepezil hybrids were designed and developed as multi-target-directed ligands against AD. Most of the derivatives displayed good to better AChE inhibitory potency and high selectivity towards BuChE.

Derivatives **9d** and **17f** displayed the best inhibitory potency with IC$_{50}$ values of 0.32 and 0.41 µM, respectively. Moreover, compound **17f** displayed good antioxidant activity ORAC-FL values of 3.3 trolox equivalents and acted as an MAO-B inhibitor (IC$_{50}$ = 8.8 µM). Both molecular docking and kinetic analysis revealed that **17f** demonstrated a mixed-type AChE inhibition, binding to both CAS and PAS of AChE. UV-vis spectrometry confirmed compounds **9d** and **17f** were good biometal chelators. Meanwhile, both the ThT assay and TEM images revealed that the compound **17f** had remarkable inhibition potency of self-induced, *hu*AChE-induced, and Cu^{2+}-induced Aβ aggregation, and could decompose self-induced and Cu^{2+}-induced Aβ$_{1-42}$ aggregation. Furthermore, compound **17f** exhibited a good neuroprotective effect and displayed high BBB permeability *in vitro*. These results declared that compound **17f** was a potential multitarget lead compound against AD. Further investigations of AD therapeutic candidates based on these results are in progress.

4. Experiment section

4.1. Chemistry

All the reaction was detected by TLC, and the purity was performed by high-performance liquid chromatography (HPLC). HPLC analysis was performed on a Shimadzu LC-10Avp plus system using a Kromasil C$_{18}$ column (4.6 × 250 mm, 5 um). ^{1}H NMR and ^{13}C NMR spectra were recorded and collected using a Variant INOVA spectrometer at 400 NMR and 100 NMR, respectively. Mass spectra were analysed and collected on Agilent-6210 TOF LC-MS Spectrometer.

4.1.1. General procedure for the synthesis of derivatives 2a–c

Compounds **2a–c** were synthesised, and their characterisation data were consistent with the reported previously.

4.1.2. General procedure for the synthesis of derivatives 3a–b

Compounds **3a–b** were synthesised referenced our previous work[27].

4.1.3. General procedure for the synthesis of derivatives 4a–b, 5a–c, and 6a–b

To a mixture of the appropriate derivatives **2a–c** (5 mmol), anhydrous K$_2$CO$_3$ (6 mmol) in CH$_3$CN (10 ml), secondary amines **3a–b**, and diethylamine (5.5 mmol) were added. The reaction mixture was heated to 65 °C for 6–8 h. After a complete reaction, the solvent was concentrated in a vacuum. Then water (30 ml) and dichloromethane (30 ml) were added, respectively, and extracted. And then saturated aqueous NaCl (30 ml) was added to wash the combined organic phases and dried with Na$_2$SO$_4$. The organic phases were evaporated and the residue was purified on a silica gel chromatography using mixtures of petroleum/acetone as eluent to obtain the oil products **4a–b**, **5a–c**, and **6a–b**.

Table 4. Inhibition potency of huMAO-A and huMAO-B) and selectivity index (SI) values of clorgyline, rasagiline, iproniazid, and chalcone-Vitamin E-donepezil hybrids.

Compds.	IC$_{50}$ (µM) ± SD[a]		SI[b]
	MAO-B	MAO-A	
8	n.t.[c]	22.9%[d]	–
16	n.t.[c]	15.4 ± 0.16	–
9a	3.8 ± 0.02	13.9%[d]	–
9b	8.1 ± 0.03	19.8 ± 0.22	2.4
9c	23.6 ± 0.12	35.7 ± 0.36	1.5
9d	12.3 ± 0.08	38.2 ± 0.63	3.1
9e	2.5 ± 0.01	37.8 ± 0.57	15.1
9f	7.2 ± 0.03	43.6 ± 0.68	6.1
10	14.6 ± 0.03	27.9 ± 0.28	1.9
17a	4.4%[d]	18.2%[d]	–
17b	2.1%[d]	14.6%[d]	–
17c	11.0%[d]	18.3 ± 0.15	–
17d	15.1 ± 0.16	16.7%[d]	–
17e	12.8 ± 0.31	17.9%[d]	–
17f	8.8 ± 0.06	37.5 ± 0.35	4.3
Clorgyline	20.8 ± 0.27	0.0027 ± 0.0001	0.0001
Rasagiline	0.0281 ± 0.0068	0.587 ± 0.038	20.9
Iproniazid	1.35 ± 0.02	5.48 ± 0.03	4.1

[a]The experiments were performed three times and the IC$_{50}$ values were expressed as the mean ± SEM.
[b]SI = selectivity index = IC$_{50}$ (hMAO-A)/IC$_{50}$ (hMAO-B).
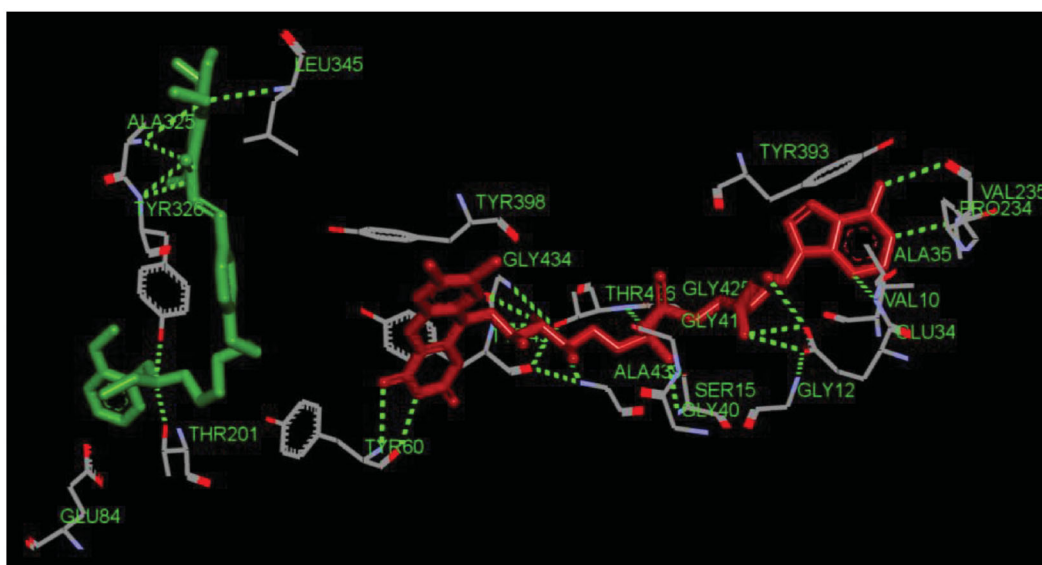[c]n.t. = not tested.
[d]Percent inhibition rate at 10 µM.

Figure 10. The interactions between compound **17f** (green stick) and the residues of the active site in *hu*MAO-B (PDB code: 2V60).
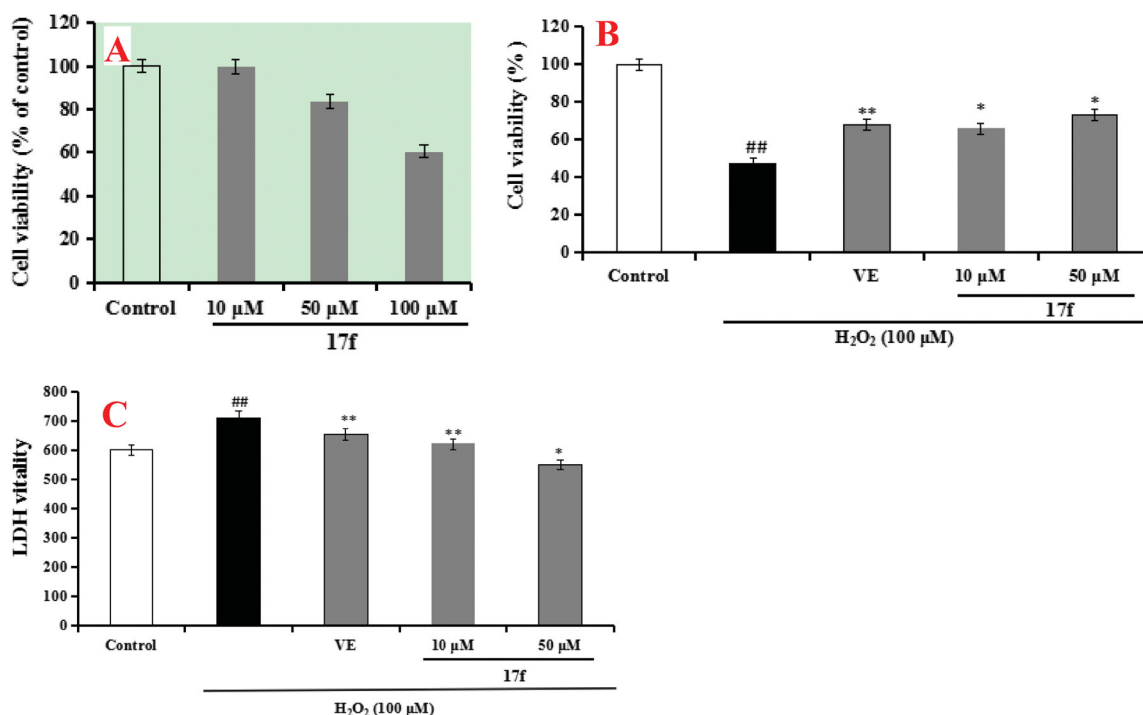
Figure 11. (A) Cytotoxicity of **17f** in PC12 cells. (B) Attenuation of H_2O_2-induced PC12 cell injury by compound **17f** was tested using MTT assay. (C) The LDH activity of compound **17f** on H_2O_2-induced PC12 cell injury was evaluated using LDH assay. Three independent experiments were carried out. Data were expressed as mean ± SD and percentage of control value. $^{\#\#}p < 0.01$ vs. control; $^{**}p < 0.01$, $^{*}p < 0.05$ vs. H_2O_2 group. VE: Vitamin E.

Table 5. The predictive penetration of **17f** by PAMPA-BBB assay.

Compounds	P_e ($\times 10^{-6}$ cm/s)	Prediction
17f	4.23 ± 0.37	CNS+
Verapamil	17.93 ± 1.26	CNS+
Diazepam	13.12 ± 0.79	CNS+
Enoxacine	0.53 ± 0.02	CNS−

4.1.3.1. 4-[[3-[Methyl(2-methoxyphenyl)methyl]amino]propyl]oxy]-benzaldehyde (4a). Intermediate **2a** was treated with N-methyl-2-methoxy-benzenemethanamine (**3a**) to obtain **4a** as colourless oil, yield 89.5%. ^{1}H NMR (400 MHz, CDCl$_3$) δ 9.88 (s, 1H), 7.82 (d, J = 8.8 Hz, 2H), 7.32 (d, J = 7.2 Hz, 1H), 7.24 (t, J = 7.2 Hz, 1H), 6.98 (d, J = 8.8 Hz, 2H), 6.90 (t, J = 7.2 Hz, 1H), 6.86 (d, J = 8.0 Hz, 1H), 4.14 (t, J = 6.4 Hz, 2H), 3.80 (s, 3H), 3.61 (s, 2H), 2.65 (t, J = 6.4 Hz, 2H), 2.30 (s, 3H), 2.11–2.07 (m, 2H).

4.1.3.2. 4-[[3-[Ethyl(2-methoxyphenyl)methyl]amino]propyl]oxy]-benzaldehyde (4b). Intermediate **2a** was treated with N-ethyl-2-methoxy-benzenemethanamine (**3b**) to obtain **4b** as colourless oil, yield 87.5%. ^{1}H NMR (400 MHz, CDCl$_3$) δ 9.88 (s, 1H), 7.81 (d, J = 8.4 Hz, 2H), 7.40 (d, J = 7.2 Hz, 1H), 7.22 (dt, J_1 = 7.6 Hz, J_2 = 1.6 Hz, 1H), 6.96 (d, J = 8.4 Hz, 2H), 6.90 (t, J = 7.2 Hz, 1H), 6.85 (d, J = 8.0 Hz, 1H), 4.10 (t, J = 6.4 Hz, 2H), 3.81 (s, 3H), 3.69 (s, 2H), 2.71 (t, J = 6.8 Hz, 2H), 2.62 (q, J_1 = 13.2 Hz, J_2 = 6.8 Hz, 2H), 2.05–2.00 (m, 2H), 1.11 (t, J = 6.8 Hz, 3H).

4.1.3.3. 4-[[4-[Methyl(2-methoxyphenyl)methyl]amino]butyl]oxy]-benzaldehyde (5a). Intermediate **2b** was treated with N-methyl-2-methoxy-benzenemethanamine (**3a**) to obtain **5a** as colourless oil, yield 85.5%. ^{1}H NMR (400 MHz, CDCl$_3$) δ 9.87 (s, 1H), 7.82 (d, J = 8.4 Hz, 2H), 7.39 (d, J = 7.2 Hz, 1H), 7.28 (t, J = 7.6 Hz, 1H), 6.96 (d, J = 8.4 Hz, 2H), 6.94 (t, J = 7.6 Hz, 1H), 6.88 (d, J = 8.4 Hz, 1H), 4.05 (t, J = 4.8 Hz, 2H), 3.83 (s, 3H), 3.74 (s, 2H), 2.67–2.62 (m, 2H), 2.37 (s, 3H), 1.90–1.84 (m, 4H).

4.1.3.4. 4-[[4-[Ethyl(2-methoxyphenyl)methyl]amino]butyl]oxy]ben-zaldehyde (5b). Intermediate **2b** was treated with N-methyl-2-ethoxy-benzenemethanamine (**3b**) to obtain **5b** as colourless oil,

yield 81.2%. ^{1}H NMR (400 MHz, CDCl$_3$) δ 9.88 (s, 1H), 7.81 (d, J = 8.4 Hz), 7.43 (d, J = 7.2 Hz, 1H), 7.22 (t, J = 7.6 Hz, 1H), 6.96 (d, J = 8.8 Hz, 2H), 6.92 (t, J = 7.2 Hz, 1H), 6.85 (d, J = 8.0 Hz, 1H), 4.02 (t, J = 6.4 Hz, 2H), 3.81 (s, 3H), 3.65 (s, 2H), 2.59–2.55 (m, 4H), 1.86–1.80 (m, 2H), 1.72–1.68 (m, 2H), 1.09 (t, J = 7.2 Hz, 3H).

4.1.3.5. 4-[3-(Diethylamino)propoxy]benzaldehyde (5c). Intermediate **2b** was treated with diethylamine to obtain **5c** as colourless oil, yield 90.5%. ^{1}H NMR (400 MHz, CDCl$_3$) δ 9.88 (s, 1H), 7.83 (d, J = 8.8 Hz, 2H), 6.99 (d, J = 8.4 Hz, 1H), 4.08 (t, J = 6.0 Hz, 2H), 2.64–2.55 (m, 6H), 1.86–1.81 (m, 2H), 1.73–1.68 (m, 2H), 1.08 (t, J = 6.8 Hz, 6H).

4.1.3.6. 4-[[6-[Methyl(2-methoxyphenyl)methyl]amino]hexyl]oxy]-benzaldehyde (6a). Intermediate **2c** was treated with N-methyl-2-methoxy-benzenemethanamine (**3a**) to obtain **6a** as colourless oil, yield 86.1%. ^{1}H NMR (400 MHz, CDCl$_3$) δ 9.88 (s, 1H), 7.82 (d, J = 8.4 Hz, 2H), 7.34 (d, J = 7.2 Hz, 1H), 7.24 (t, J = 7.6 Hz, 1H), 6.98 (d, J = 8.8 Hz, 2H), 6.93 (t, J = 7.2 Hz, 1H), 6.87 (d, J = 8.0 Hz, 1H), 4.03 (t, J = 6.4 Hz, 2H), 3.82 (s, 3H), 3.57 (s, 2H), 2.45 (t, J = 6.8 Hz, 2H), 2.25 (t, J = 6.8 Hz, 2H), 1.84–1.79 (m, 2H), 1.63–1.57 (m, 2H), 1.51–1.46 (m, 2H), 1.43–1.40 (m, 2H).

4.1.3.7. 4-[[6-[Ethyl(2-methoxyphenyl)methyl]amino]hexyl]oxy]ben-zaldehyde (6b). Intermediate **2c** was treated with N-ethyl-2-methoxy-benzenemethanamine (**3b**) to obtain **6b** as colourless oil, yield 87.6%. ^{1}H NMR (400 MHz, CDCl$_3$) δ 9.87 (s, 1H), 7.82 (d, J = 8.4 Hz, 2H), 7.47 (d, J = 6.4 Hz, 1H), 7.24 (t, J = 7.6 Hz, 1H), 6.97 (d, J = 8.8 Hz, 2H), 6.94 (t, J = 7.2 Hz, 1H), 6.86 (d, J = 8.0 Hz, 1H), 4.01 (t, J = 6.4 Hz, 2H), 3.82 (s, 3H), 3.72 (s, 2H), 2.65–2.63 (m, 2H), 2.58–2.54 (m, 2H), 1.83–1.76 (m, 2H), 1.63–1.60 (m, 2H), 1.50–1.43 (m, 2H), 1.40–1.33 (m, 2H), 1.12 (t, J = 7.2 Hz, 3H).

4.1.4. 1-[6-Hydroxy-2,4-dimethoxy-3-(methoxymethoxy)phenyl]e-thanone (12)

A mixture of material **11** (5 mmol) and (i-Pr)$_2$EtN (6 mmol) in acetone 20 ml and chloromethyl methyl ether (5.5 mmol) was added

slowly at −5 °C for 0.5 h. Then the mixture was heated at 50 °C for 6–8 h. Finally, the solvents were evaporated, then water (30 ml) and dichloromethane (30 ml) were added, respectively, and extracted. And then saturated aqueous NaCl (30 ml) was added to wash the combined organic phases and dried with Na_2SO_4. The organic phases were evaporated and the residue was purified by column chromatography on silica gel (petroleum/acetone as eluent) to obtain the colourless oil product **12** as colourless oil, yield 67.3%. ^1H NMR (400 MHz, $CDCl_3$) δ 13.43 (s, 1H), 5.02 (s, 2H), 3.96 (s, 3H), 3.88 (s, 3H), 3.61 (s, 3H), 2.66 (s, 3H).

4.1.5. General procedure for the synthesis of 8, 9a–f, 10, 13a–b, 14a–b, and 15a–b

The acetophenone derivatives (1 mmol) were reacted with the appropriate benzaldehyde derivatives (1 mmol) in EtOH (3 ml) by slowly adding 50% KOH (4 mmol). After for 72 h to 100 h reaction, 10% HCl was added to adjust pH = 2, and then added NaHCO₃ powder to the mixture, and then extracted with CH_2Cl_2 (10 ml × 3). Then the organic phase was washed using aqueous NaHCO₃ (30 ml × 2) and aqueous NaCl (30 ml) and dried with Na₂SO₄. Finally, the organic phase was evaporated and the residue was purified on a silica gel chromatography by mixtures of CH_2Cl_2/acetone as eluent to get target derivatives **8**, **9a–f**, **10**, **13a–b**, **14a–b**, and **15a–b**.

4.1.5.1. (E)-1-(6-hydroxy-2,3,4-trimethoxy-phenyl)-3-(4-hydroxy-phenyl)-2-propen-1-one (8). Material **7** was treated with p-hydroxy-benzaldehyde to obtain **8** as yellow solid, 61.5% yield, mp: 142.2–143.2 °C. ^1H NMR (400 MHz, $CDCl_3$) δ 13.78 (s, 1H), 7.85 (d, $J=16.0$ Hz, 1H), 7.80 (d, $J=16.0$ Hz, 1H), 7.56 (d, $J=8.4$ Hz, 2H), 6.88 (d, $J=8.4$ Hz, 2H), 6.30 (s, 1H), 5.37 (brs, 1H), 3.93 (s, 3H), 3.90 (s, 3H), 3.84 (s, 3H).

4.1.5.2. (E)-1-(6-Hydroxy-2,3,4-trimethoxyphenyl)-3-(4-(3-((2-methoxybenzyl)(methyl)amino)propoxy)phenyl)prop-2-en-1-one (9a). Material **7** was treated with intermediate **4a** to obtain **9a** as yellow oil, 50.5% yield, 98.4% HPLC purity. ^1H NMR (400 MHz, $CDCl_3$) δ 13.78 (s, 1H), 7.86 (d, $J=16.0$ Hz, 1H), 7.82 (d, $J=16.0$ Hz, 1H), 7.59 (d, $J=8.4$ Hz, 2H), 7.42–7.38 (m, 1H), 7.29–7.26 (m, 1H), 6.99–6.88 (m, 4H), 6.30 (s, 1H), 4.11 (t, $J=6.0$ Hz, 2H), 3.93 (s, 3H), 3.91 (s, 3H), 3.84 (s, 3H), 3.83 (s, 3H), 3.72 (brs, 2H), 2.78–2.75 (m, 2H), 2.39 (s, 3H), 2.19–2.16 (m, 2H). MS (ESI) m/z: 522.2 $[M+H]^+$.

4.1.5.3. (E)-3-(4-(3-(ethyl(2-methoxybenzyl)amino)propoxy)phenyl)-1-(6-hydroxy-2,3,4-trimethoxyphenyl)prop-2-en-1-one (9b). Material **7** was treated with intermediate **4b** to obtain **9b** as yellow oil, 60.5% yield, 97.9% HPLC purity. ^1H NMR (400 MHz, $CDCl_3$) δ 13.80 (s, 1H), 7.86 (d, $J=16.0$ Hz, 1H), 7.82 (d, $J=16.0$ Hz, 1H), 7.58 (d, $J=8.8$ Hz, 2H), 7.40 (d, $J=6.8$ Hz, 1H), 7.21 (t, $J=7.6$ Hz, 1H), 6.92–6.89 (m, 3H), 6.85 (d, $J=8.0$ Hz, 1H), 6.30 (s, 1H), 4.07 (t, $J=6.4$ Hz, 2H), 3.93 (s, 3H), 3.90 (s, 3H), 3.84 (s, 3H), 3.81 (s, 3H), 3.64 (s, 2H), 2.69–2.65 (m, 2H), 2.58–2.55 (m, 2H), 2.01–1.95 (m, 2H), 1.07 (t, $J=6.4$ Hz, 3H). ^{13}C NMR (100 MHz, $CDCl_3$) δ 192.72, 162.54, 161.09, 159.80, 157.56, 154.88, 143.50, 135.18, 131.85, 130.13, 130.02, 127.72, 123.65, 120.20, 114.84, 114.66, 110.11, 108.67, 96.49, 66.29, 61.83, 61.20, 55.80, 55.19, 51.36, 49.59, 47.72, 26.79, 11.72. MS (ESI) m/z: 536.3 $[M+H]^+$.

4.1.5.4. (E)-1-(6-hydroxy-2,3,4-trimethoxyphenyl)-3-(4-(4-((2-methoxybenzyl)(methyl)amino)butoxy)phenyl)prop-2-en-1-one (9c). Material **7** was treated with intermediate **5a** to obtain **9c** as yellow oil, 60.5% yield, 98.5% HPLC purity. ^1H NMR (400 MHz, $CDCl_3$) δ 13.79 (s, 1H), 7.87 (d, $J=15.6$ Hz, 1H), 7.82 (d, $J=15.6$ Hz, 1H), 7.59 (d, $J=9.2$ Hz, 2H), 7.44–7.40 (m, 1H), 7.29 (t, $J=7.2$ Hz, 1H), 6.96 (t, $J=7.6$ Hz, 1H), 6.92–6.89 (m, 3H), 6.30 (s, 1H), 4.03 (t, $J=6.0$ Hz, 2H), 3.93 (s, 3H), 3.91 (s, 3H), 3.85 (s, 3H), 3.84 (s, 3H), 3.82 (s, 2H), 2.75–2.72 (m, 2H), 2.45–2.41 (m, 2H), 1.90–1.85 (m, 4H). ^{13}C NMR (100 MHz, $CDCl_3$) δ 192.79, 162.58, 160.94, 159.88, 157.87, 154.94, 143.44, 135.24, 131.37, 130.21, 129.03, 127.91, 123.85, 120.47, 114.87, 110.51, 108.72, 96.53, 67.68, 61.90, 61.27, 56.57, 56.05, 55.40, 54.76, 41.58, 26.85, 23.08. MS (ESI) m/z: 536.3 $[M+H]^+$.

4.1.5.5. (E)-3-(4-(4-(ethyl(2-methoxybenzyl)amino)butoxy)phenyl)-1-(6-hydroxy-2,3,4-trimethoxyphenyl)prop-2-en-1-one (9d). Material **7** was treated with intermediate **5b** to obtain **9d** as yellow oil, 60.5% yield, 98.1% HPLC purity. ^1H NMR (400 MHz, $CDCl_3$) δ 13.78 (s, 1H), 7.86 (d, $J=16.0$ Hz, 1H), 7.82 (d, $J=16.0$ Hz, 1H), 7.58 (d, $J=8.4$ Hz, 2H), 7.48 (d, $J=6.8$ Hz, 1H), 7.26 (t, $J=7.2$ Hz, 1H), 6.95 (t, $J=8.0$ Hz, 1H), 6.91–6.86 (m, 3H), 6.30 (s, 1H), 4.00 (t, $J=5.6$ Hz, 2H), 3.93 (s, 3H), 3.90 (s, 3H), 3.84 (s, 3H), 3.83 (s, 3H), 3.79 (s, 2H), 2.70–2.65 (m, 4H), 1.84–1.79 (m, 4H), 1.18 (t, $J=6.4$ Hz). MS (ESI) m/z: 550.3 $[M+H]^+$.

4.1.5.6. (E)-1-(6-hydroxy-2,3,4-trimethoxyphenyl)-3-(4-(6-((2-methoxybenzyl)(methyl)amino)hexyloxy)phenyl)prop-2-en-1-one (9e). Material **7** was treated with intermediate **6a** to obtain **9e** as yellow oil, 45.5% yield, 98.7% HPLC purity. ^1H NMR (400 MHz, $CDCl_3$) δ 13.79 (s, 1H), 7.86 (d, $J=16.0$ Hz, 1H), 7.82 (d, $J=16.0$ Hz, 1H), 7.59 (d, $J=8.8$ Hz, 2H), 7.37 (d, $J=4.8$ Hz, 1H), 7.26 (t, $J=6.8$ Hz, 1H), 6.96–6.87 (m, 4H), 6.30 (s, 1H), 4.00 (t, $J=6.8$ Hz, 2H), 3.93 (s, 3H), 3.90 (s, 3H), 3.84 (s, 3H), 3.83 (s, 3H), 3.65 (s, 2H), 2.54–2.50 (m, 2H), 2.30 (s, 3H),1.83–1.78 (m, 2H), 1.68–1.63 (m, 2H), 1.50–1.46 (m, 2H), 1.44–1.40 (m, 2H). ^{13}C NMR (100 MHz, $CDCl_3$) δ 192.67, 162.48, 160.96, 159.78, 157.70, 154.82, 143.36, 135.13, 131.41, 130.11, 129.20, 127.71, 123.68, 120.60, 114.77, 114.58, 110.35, 108.60, 96.42, 67.78, 61.78, 61.16, 55.95, 55.29, 52.33, 50.51, 47.17, 28.78, 26.85, 25.63, 25.23, 10.40. MS (ESI) m/z: 564.3 $[M+H]^+$.

4.1.5.7. (E)-3-(4-(6-(ethyl(2-methoxybenzyl)amino)hexyloxy)phenyl)-1-(6-hydroxy-2,3,4-trimethoxyphenyl)prop-2-en-1-one (9f). Material **7** was treated with intermediate **6b** to obtain **9f** as yellow oil, 63.5% yield, 97.6% HPLC purity. ^1H NMR (400 MHz, $CDCl_3$) δ 13.79 (s, 1H), 7.86 (d, $J=16.0$ Hz, 1H), 7.82 (d, $J=16.0$ Hz, 1H), 7.60–7.55 (m, 3H), 7.30 (t, $J=6.8$ Hz, 1H), 6.99 (t, $J=6.8$ Hz, 1H), 6.93–6.88 (m, 3H), 6.30 (s, 1H), 3.99 (t, $J=6.4$ Hz, 2H), 3.93 (s, 3H), 3.90 (s, 3H), 3.84 (s, 3H), 3.83 (s, 3H), 3.87 (s, 2H), 2.78–2.71 (m, 4H), 1.83 (m, 4H), 1.51–1.45 (m, 2H), 1.41–1.36 (m, 2H), 1.26–1.21 (m, 3H). MS (ESI) m/z: 578.3 $[M+H]^+$.

4.1.5.8. (E)-3-(4-(4-(diethylamino)butoxy)phenyl)-1-(6-hydroxy-2,3,4-trimethoxyphenyl)prop-2-en-1-one (10). Material **7** was treated with intermediate **5c** to obtain **10** as yellow oil, 60.3% yield, 98.2% HPLC purity. ^1H NMR (400 MHz, $CDCl_3$) δ 13.77 (s, 1H), 7.87 (d, $J=15.6$ Hz, 1H), 7.82 (d, $J=15.6$ Hz, 1H), 7.60 (d, $J=8.8$ Hz, 2H), 6.92 (d, $J=8.8$ Hz, 2H), 4.06 (t, $J=5.6$ Hz, 2H), 3.95 (s, 3H), 3.93 (s, 3H), 3.84 (s, 3H), 2.94–2.83 (m, 8H), 1.93–1.84 (m, 4H), 1.28 (t, $J=6.8$ Hz, 6H). ^{13}C NMR (100 MHz, $CDCl_3$) δ 192.55, 162.38, 160.51, 159.74, 154.71, 143.09, 135.03, 130.03, 127.86, 123.78, 114.66, 108.46, 96.31, 67.11, 61.69, 61.07, 55.88, 51.31, 46.36, 26.52, 21.42, 9.54. MS (ESI) m/z: 458.3 $[M+H]^+$.

4.1.5.9. (E)-1-(6-hydroxy-2,4-dimethoxy-3-(methoxymethyl)-phenyl)-3-(4-(3-((2-methoxybenzyl)(methyl)amino)propoxy)phenyl)-prop-2-en-1-one (13a). Compound **12** was treated with intermediate **4a** to obtain **13a** as yellow oil, 51.2% yield. ^1H NMR (400 MHz, $CDCl_3$) δ 13.80 (s, 1H), 7.87 (d, $J=15.6$ Hz, 1H), 7.82 (d, $J=15.6$ Hz, 1H), 7.58 (d, $J=8.8$ Hz, 2H), 7.32 (d, $J=7.6$ Hz, 1H), 7.23 (t, $J=8.0$ Hz, 1H), 6.93–6.89 (m, 3H), 6.86 (d, $J=8.0$ Hz, 1H), 6.31 (s, 1H), 5.08 (s, 2H), 4.10 (t, $J=6.4$ Hz, 2H), 3.89 (s, 3H), 3.89 (s, 3H), 3.81 (s, 3H), 3.64 (s, 3H), 3.59 (s, 2H), 2.64 (t, $J=6.8$ Hz, 2H), 2.29 (s, 3H), 2.08–2.05 (m, 2H).

4.1.5.10. (E)-3-(4-(3-(ethyl(2-methoxybenzyl)amino)propoxy)-phenyl)-1-(6-hydroxy-2,4-dimethoxy-3-(methoxymethyl)phenyl)prop-

2-en-1-one (**13b**). Compound **12** was treated with intermediate **4b** to obtain **13b** as yellow oil, 51.2% yield. ¹H NMR (400 MHz, CDCl₃) δ 13.79 (s, 1H), 7.87 (d, J = 15.6 Hz, 1H), 7.83 (d, J = 15.6 Hz, 1H), 7.57 (d, J = 8.4 Hz, 2H), 7.41 (d, J = 6.8 Hz, 1H), 7.22 (t, J = 8.0 Hz, 1H), 6.93–6.89 (m, 3H), 6.85 (d, J = 8.0 Hz, 1H), 6.31 (s, 1H), 5.08 (s, 2H), 4.07 (t, J = 6.4 Hz, 2H), 3.89 (s, 3H), 3.89 (s, 3H), 3.81 (s, 3H), 3.67 (s, 2H), 3.64 (s, 3H), 2.74–2.65 (m, 2H), 2.63–2.58 (m, 2H), 2.04–2.00 (m, 2H), 1.09 (t, J = 6.8 Hz, 3H).

4.1.5.11. *(E)-1-(6-hydroxy-2,4-dimethoxy-3-(methoxymethyl)-phenyl)-3-(4-(4-((2-methoxybenzyl)(methyl)amino)butoxy)phenyl)prop-2-en-1-one (**14a**).* Compound **12** was treated with intermediate **5a** to obtain **14a** as yellow oil, 58.3% yield. ¹H NMR (400 MHz, CDCl₃) δ 13.79 (s, 1H), 7.87 (d, J = 16.0 Hz, 1H), 7.83 (d, J = 16.0 Hz, 1H), 7.58 (d, J = 8.4 Hz, 2H), 7.44–7.36 (m, 1H), 7.29–7.26 (m, 1H), 6.96–6.88 (m, 4H), 6.31 (s, 1H), 5.08 (s, 2H), 4.03 (t, J = 5.2 Hz, 2H), 3.89 (s, 3H), 3.89 (s, 3H), 3.83 (s, 3H), 3.64 (s, 2H), 3.61 (s, 3H), 2.62–2.58 (m, 2H), 2.36–2.31 (m, 3H), 1.87–1.83 (m, 4H).

4.1.5.12. *(E)-3-(4-(4-(ethyl(2-methoxybenzyl)amino)butoxy)phenyl)-1-(6-hydroxy-2,4-dimethoxy-3-(methoxymethyl)phenyl)prop-2-en-1-one (**14b**).* Compound **12** was treated with intermediate **5b** to obtain **14b** as yellow oil, 51.2% yield. ¹H NMR (400 MHz, CDCl₃) δ 13.78 (s, 1H), 7.87 (d, J = 16.0 Hz, 1H), 7.82 (d, J = 16.0 Hz, 1H), 7.62–7.54 (m, 3H), 7.34 (t, J = 8.0 Hz, 1H), 6.98 (t, J = 7.2 Hz, 1H), 6.92–6.88 (m, 3H), 6.31 (s, 1H), 5.07 (s, 2H), 4.06 (s, 2H), 4.01 (t, J = 6.0 Hz, 2H), 3.89 (s, 3H), 3.88 (s, 3H), 3.86 (s, 3H), 3.64 (s, 3H), 2.92–2.85 (m, 4H), 2.01–1.96 (m, 2H), 1.87–1.82 (m, 2H), 1.33 (t, J = 6.8 Hz, 3H).

4.1.5.13. *(E)-1-(6-hydroxy-2,4-dimethoxy-3-(methoxymethyl)-phenyl)-3-(4-(6-((2-methoxybenzyl)(methyl)amino)hexyloxy)phenyl)-prop-2-en-1-one (**15a**).* Compound **12** was treated with intermediate **6a** to obtain **15a** as yellow oil, 48.3% yield. ¹H NMR (400 MHz, CDCl₃) δ 13.79 (s, 1H), 7.87 (d, J = 16.0 Hz, 1H), 7.83 (d, J = 16.0 Hz, 1H), 7.59 (d, J = 8.8 Hz, 2H), 7.47 (d, J = 6.8 Hz, 1H), 7.33 (t, J = 7.2 Hz, 1H), 6.99 (t, J = 7.2 Hz, 1H), 6.93–6.90 (m, 3H), 6.31 (s, 1H), 5.08 (s, 2H), 4.00 (t, J = 6.0 Hz, 2H), 3.89 (s, 3H), 3.89 (s, 3H), 3.87 (s, 2H), 3.85 (s, 3H), 3.64 (s, 3H), 2.72–2.76 (m, 2H), 2.45 (s, 3H), 1.85–1.78 (m, 4H), 1.55–1.48 (m, 2H), 1.43–1.39 (m, 2H).

4.1.5.14. *(E)-3-(4-(6-(ethyl(2-methoxybenzyl)amino)hexyloxy)-phenyl)-1-(6-hydroxy-2,4-dimethoxy-3-(methoxymethyl)phenyl)prop-2-en-1-one (**15b**).* Compound **12** was treated with intermediate **6b** to obtain **15b** as yellow oil, 54.1% yield. ¹H NMR (400 MHz, CDCl₃) δ 13.80 (s, 1H), 7.87 (d, J = 16.0 Hz, 1H), 7.83 (d, J = 16.0 Hz, 1H), 7.62 (d, J = 7.6 Hz, 1H), 7.59 (d, J = 8.8 Hz, 2H), 7.36 (t, J = 7.2 Hz, 1H), 7.01 (t, J = 7.6 Hz, 1H), 6.93–6.90 (m, 3H), 6.31 (s, 1H), 5.08 (s, 2H), 4.09 (s, 2H), 3.99 (t, J = 6.4 Hz, 2H), 3.89 (s, 3H), 3.89 (s, 3H), 3.86 (s, 3H), 3.64 (s, 3H), 2.95–2.91 (m, 2H), 2.86–2.81 (m, 2H), 1.83–1.77 (m, 4H), 1.52–1.47 (m, 2H), 1.42–1.38 (m, 2H), 1.33–1.31 (m, 3H).

4.1.5.15. *3′,4,6′-Trihydroxy-2′,4′-dimethoxy-chalcone (**16**).* Compound **11** was treated with p-hydroxybenzaldehyde to obtain **16** as yellow oil, 24.3% yield. ¹H NMR (400 MHz, CDCl₃) δ 13.38 (s, 1H), 7.86 (d, J = 15.2 Hz, 1H), 7.82 (d, J = 15.2 Hz, 1H), 7.56 (d, J = 8.4 Hz, 1H), 6.88 (d, J = 8.8 Hz, 2H), 6.33 (s, 1H), 5.66 (brs, 1H), 3.95 (s, 3H), 3.87 (s, 3H).

4.1.6. General procedure for the synthesis of 17a–f

A mixture of intermediates **13a–b**, **14a–b**, and **15a–b** (1.5 mmol) in EtOH (1 ml) was added 10% HCl (1 ml) for 24 h at room temperature. And then the mixture was adjusted pH = 8 using NaHCO₃ powder and extracted with CH₂Cl₂ (10 ml × 3). The organic phases were washed with 30 ml saturated aqueous NaCl and dried with Na₂SO₄. Finally, the solvent was evaporated and

the residue was purified using mixtures of CH₂Cl₂/acetone as eluent to obtain products **17a–f**.

4.1.6.1. *(E)-1-(3,6-dihydroxy-2,4-dimethoxyphenyl)-3-(4-(3-((2-methoxybenzyl)(methyl)amino)propoxy)phenyl)prop-2-en-1-one (**17a**).* Compound **13a** was treated with 10% HCl to obtain **17a** as orange oil, 87.2% yield, 98.3% HPLC purity. ¹H NMR (400 MHz, CDCl₃) δ 13.41 (s, 1H), 7.87 (d, J = 15.2 Hz, 1H), 7.83 (d, J = 15.2 Hz, 1H), 7.58 (d, J = 8.4 Hz, 1H), 7.32 (d, J = 7.2 Hz, 1H), 7.23 (t, J = 8.0 Hz, 1H), 6.92 (d, J = 8.8 Hz, 1H), 6.88–6.84 (m, 2H), 6.32 (s, 1H), 5.32 (brs, 1H), 4.10 (t, J = 6.4 Hz, 2H), 3.94 (s, 3H), 3.87 (s, 3H), 3.80 (s, 3H), 3.57 (s, 2H), 2.62 (t, J = 6.8 Hz, 2H), 2.28 (s, 3H), 2.09–2.02 (m, 2H). MS (ESI) m/z: 508.2 [M + H]⁺.

4.1.6.2. *(E)-1-(3,6-dihydroxy-2,4-dimethoxyphenyl)-3-(4-(3-(ethyl(2-methoxybenzyl)amino)propoxy)phenyl)prop-2-en-1-one (**17b**).* Compound **13b** was treated with 10% HCl to obtain **17b** as orange oil, 81.6% yield, 97.8% HPLC purity. ¹H NMR (400 MHz, CDCl₃) δ 13.41 (s, 1H), 7.87 (d, J = 15.2 Hz, 1H), 7.83 (d, J = 15.2 Hz, 1H), 7.58 (d, J = 8.8 Hz, 1H), 7.44–7.41 (m, 1H), 7.23 (t, J = 8.0 Hz, 1H), 6.94–6.84 (m, 4H), 6.33 (s, 1H), 5.22 (brs, 1H), 4.07 (t, J = 6.0 Hz, 2H), 3.94 (s, 3H), 3.87 (s, 3H), 3.78 (s, 3H), 3.59 (s, 2H), 2.69–2.61 (m, 4H), 2.02–2.00 (m, 2H), 1.02–1.00 (m, 3H). ¹³C NMR (100 MHz, CDCl₃) δ 192.46, 160.99, 159.47, 157.61, 154.26, 146.95, 143.54, 131.76, 130.40, 130.13, 128.11, 127.67, 123.40, 120.26, 114.82, 110.17, 108.46, 96.05, 66.18, 61.67, 56.11, 55.19, 51.15, 49.49, 47.60, 26.41, 11.35. MS (ESI) m/z: 522.2 [M + H]⁺.

4.1.6.3. *(E)-1-(3,6-dihydroxy-2,4-dimethoxyphenyl)-3-(4-(4-((2-methoxybenzyl)(methyl)amino)butoxy)phenyl)prop-2-en-1-one (**17c**).* Compound **14a** was treated with 10% HCl to obtain **17c** as orange oil, 85.8% yield, 98.0% HPLC purity. ¹H NMR (400 MHz, CDCl₃) δ 13.41 (s, 1H), 7.87 (d, J = 15.2 Hz, 1H), 7.83 (d, J = 15.2 Hz, 1H), 7.58 (d, J = 8.4 Hz, 1H), 7.39 (d, J = 6.8 Hz, 1H), 7.28 (t, J = 8.0 Hz, 1H), 6.96–6.87 (m, 4H), 6.33 (s, 1H), 5.25 (brs, 1H), 4.02 (t, J = 5.6 Hz, 2H), 3.94 (s, 3H), 3.87 (s, 3H), 3.83 (s, 3H), 3.70 (s, 2H), 2.62–2.60 (m, 2H), 2.34 (s, 3H), 1.86–1.84 (m, 4H). ¹³C NMR (100 MHz, CDCl₃) δ 192.53, 161.01, 159.55, 157.87, 154.20, 146.93, 143.57, 131.77, 131.32, 130.23, 128.90, 127.83, 123.52, 120.42, 114.89, 110.48, 108.54, 96.13, 67.72, 61.80, 56.62, 56.22, 55.37, 54.79, 41.65, 26.88, 23.15. MS (ESI) m/z: 522.2 [M + H]⁺.

4.1.6.4. *(E)-1-(3,6-dihydroxy-2,4-dimethoxyphenyl)-3-(4-(4-(ethyl(2-methoxybenzyl)amino)butoxy)phenyl)prop-2-en-1-one (**17d**).* Compound **14b** was treated with 10% HCl to obtain **17d** as orange oil, 82.9% yield, 97.8% HPLC purity. ¹H NMR (400 MHz, CDCl₃) δ 13.40 (s, 1H), 7.87 (d, J = 15.2 Hz, 1H), 7.83 (d, J = 15.2 Hz, 1H), 7.59–7.56 (m, 3H), 7.31 (t, J = 8.0 Hz, 1H), 6.97 (t, J = 7.6 Hz, 1H), 6.91–6.87 (m, 3H), 6.33 (s, 1H), 5.23 (brs, 1H), 4.01 (t, J = 6.0 Hz, 2H), 3.98 (s, 2H), 3.94 (s, 3H), 3.91 (s, 3H), 3.87 (s, 3H), 2.79–2.77 (m, 4H), 1.84–1.82 (m, 4H), 1.26–1.24 (m, 3H). MS (ESI) m/z: 536.3 [M + H]⁺.

4.1.6.5. *(E)-1-(3,6-dihydroxy-2,4-dimethoxyphenyl)-3-(4-((6-((2-methoxybenzyl)(methyl)amino)hexyl)oxy)phenyl)prop-2-en-1-one (**17e**).* Compound **15a** was treated with 10% HCl to obtain **17e** as orange oil, 87.2% yield, 97.7% HPLC purity. ¹H NMR (400 MHz, CDCl₃) δ 13.40 (s, 1H), 7.87 (d, J = 15.2 Hz, 1H), 7.83 (d, J = 15.2 Hz, 1H), 7.59 (d, J = 8.0 Hz, 2H), 7.50 (d, J = 6.0 Hz, 1H), 7.37 (t, J = 7.2 Hz, 1H), 7.01 (t, J = 7.6 Hz, 1H), 6.94–6.90 (m, 3H), 6.33 (s, 1H), 5.23 (brs, 1H), 4.05 (s, 2H), 4.00 (t, J = 5.6 Hz, 2H), 3.94 (s, 3H), 3.87 (s, 6H), 2.83–2.80 (m, 2H), 2.55 (s, 3H), 1.84–1.82 (m, 4H), 1.53–1.50 (m, 2H), 1.44–1.41 (m, 2H). MS (ESI) m/z: 550.3 [M + H]⁺.

4.1.6.6. *(E)-1-(3,6-dihydroxy-2,4-dimethoxyphenyl)-3-(4-((6-(ethyl(2-methoxybenzyl)amino)hexyl)oxy)phenyl)prop-2-en-1-one (**17f**).* Compound **15b** was treated with 10% HCl to obtain **17f** as orange oil, 80.6% yield, 98.1% HPLC purity. ¹H NMR (400 MHz, CDCl₃) δ 13.42 (s, 1H), 7.86 (d, J = 16.0 Hz, 1H), 7.82 (d, J = 16.0 Hz,

1H), 7.57 (d, $J = 8.4$ Hz, 2H), 7.52 (d, $J = 6.4$ Hz, 1H), 7.29–7.25 (m, 1H), 6.96 (t, $J = 7.6$ Hz, 1H), 6.91–6.86 (m, 3H), 6.31 (s, 1H), 5.26 (brs, 1H), 3.98 (t, $J = 6.4$ Hz, 2H), 3.94 (s, 3H), 3.85 (s, 3H), 3.83 (s, 3H), 3.82 (s, 2H), 2.73–2.71 (m, 2H), 2.65–2.62 (m, 2H), 1.80–1.76 (m, 2H), 1.68–1.66 (m, 2H), 1.49–1.43 (m, 2H), 1.39–1.34 (m, 2H), 1.19 (t, $J = 6.4$ Hz, 3H). ^{13}C NMR (100 MHz, CDCl$_3$) δ 192.42, 160.98, 159.43, 157.69, 154.25, 146.96, 143.43, 131.77, 131.32, 130.80, 130.10, 129.04, 127.64, 127.53, 123.40, 120.51, 114.77, 110.31, 108.40, 95.98, 67.79, 61.60, 56.07, 55.25, 52.36, 50.52, 47.13, 28.87, 26.87, 25.63, 25.30, 10.46. MS (ESI) m/z: 564.3 $[M + H]^+$.

4.2. Biological assay

4.2.1. Ache and BuChE inhibition assay
The *rat*AChE was from 5% rat cortex homogenate, *rat*BuChE was from rat serum, and *ee*AChE was from electric eel (Sigma–Aldrich Co.). The tested method applied Ellman assay and the detailed procedure could reference our previous work[27,28].

4.2.2. Molecular docking
The crystal structure of the AChE complexed with donepezil (code ID: 1EVE) was obtained from the Protein Data Bank after eliminating the original inhibitors and water molecules. The 3 D Structure of **17f** was built and performed geometry optimisation by molecular mechanics. After the addition of Gasteiger charges, removal of hydrogen atoms, the addition of their atomic charges to skeleton atoms, and the assignment of proper atomic types, the further preparation of the inhibitor was accomplished. Autotors were then used to define the rotatable bonds in the ligands. Docking studies were performed using the AUTODOCK 4.2 program. By using Autodock Tools (ADT; version 1.5.6), polar hydrogen atoms were added to amino acid residues, and Gasteiger charges were assigned to all atoms of the enzyme. The resulting enzyme structure was used as an input for the AUTOGRID program. AUTOGRID performed pre-calculated atomic affinity grid maps for each atom type in the ligand, plus an electrostatics map and a separate desolvation map presented in the substrate molecule. All maps were calculated with 0.375 Å spacing between grid points. The centre of the grid box was placed at the centre of donepezil with coordinates $x = 2.023$, $y = 63.295$, $z = 67.062$. The dimensions of the active site box were set at $50 \times 50 \times 50$ Å. Flexible ligand docking was performed for the compounds. Each docked system was performed by 100 runs of the AUTODOCK search by the Lamarckian genetic algorithm (LGA). Other than the referred parameters above, the other parameters were accepted as default. A cluster analysis was performed on the docking results using a root mean square (RMS) tolerance of 1.0 and the lowest energy conformation of the highest populated cluster was selected for analysis. Graphic manipulations and visualisations were done by Autodock Tools or Discovery Studio 2.1 software[27,28].

4.2.3. Propidium iodide displacement assay
Propidium iodide displacement assay was applied to determine the binding of compound **17f** to the peripheral site of AChE by competitively displacing the propidium iodide[32–34]. The assay mixture of *ee*AChE (5 U) was incubated with or without test compound **17f** (final concentration 10 and 50 μM, 150 μl) for 6 h at 25 °C. After incubation, propidium iodide (final concentration 1 μM, 50 μl) was added to make the final assay volume of 200 μl. After 10 min, fluorescence intensity was measured at excitation and emission wavelength of $\lambda_{\text{ex}} = 535$ nm and $\lambda_{\text{em}} = 595$ nm,

respectively using Varioskan Flash Multimode Reader (PerkinElmer). The percentage inhibition was calculated by the following expression: $100 - (\text{IF}_i/\text{IF}_0 \times 100)$, where IF_i and IF_0 are the fluorescence intensities with and without inhibitor, respectively. Each assay was performed in triplicates, as three separate experiments.

4.2.4. Molecular dynamics simulations
AMBER16 was used for solvation, molecular dynamics simulation, and trajectory analysis. During the simulation, the SHAKE method was used to constrain the expansion and contraction of the chemical bond connected to the hydrogen atom, the simulation integration step was set to 2 fs, and the PME method was used to calculate the long-range electrostatic interaction, and the periodic boundary conditions (PBC) were used to eliminate the edge effect of the solvent box. The following protocols were implemented for each system: (1) The limiting potential of the proteins, ligands, and counter ions were all restricted by a force constant of 200 kcal/mol Å^2, and the energy of the solvent water molecules was minimised to make the water molecules reach a relaxed state; (2) the restriction potential for the proteins and ligands were both constrained by a force constant of 300 kcal/mol Å^2, which further minimised the energy of the system; (3) the restriction potential of the protein backbone was restricted by a force constant of 20 kcal/mol Å^2, and only the side chain was allowed to relax and minimise the energy; (4) Restrictions were not imposed on the entire system and the energy was minimised. The NPT ensemble (Isotherm and Isobaric) to heat from 10 to 300 K with constant volume during 100 ps to ensure that the system reached equilibrium. Finally, with constant temperature and pressure, an unconstrained molecular dynamics simulation of 50 ns was performed. The MMGBSA and residue-free energy decomposition calculations were made based on the generated trajectory. The whole simulation process used CUDA8.0 software to support the GPU acceleration work[31,32].

4.2.5. Metal binding studies
The metal chelation property was studied by Shimadzu UV-2450 spectrophotometer using CuCl$_2$, ZnCl$_2$, FeSO$_4$, and AlCl$_3$ at 200–600 nm. Moreover, stoichiometry was investigated by titrating the solution of derivatives with increasing CuCl$_2$. The procedure referenced our previous work[29,30].

4.2.6. Antioxidant activity assay
The ORAC-FL assay was employed to determine the antioxidant potency and referenced our previous work[29,30].

4.2.7. Effect of test compounds on self-induced $A\beta_{1-42}$ aggregation assay
The inhibition and disaggregation experiments towards self- and Cu^{2+}-mediated $A\beta_{1-42}$ aggregation were performed using ThT fluorescence assay. The detailed procedure is described in the previous work[25,29,30].

4.2.8. Inhibition of monoamine oxidase
The recombinant huMAO-A and huMAO-B were obtained from Sigma–Aldrich. All enzymatic reactions were quantified on a Varioskan Flash Multimode Reader (PerkinElmer) and the detailed experiments referenced our previous work[23,24].

Disclosure statement

Author contributions

Zhipei Sang, Yong Deng, and Li Zhang originated the concept and design. Zhipei Sang was responsible for synthesis, evaluation of *in vitro*, data analysis, and wrote the manuscript. Qing Song and Zhongcheng Cao were responsible for the synthesis of target compounds and evaluation *in vitro*.

Funding

References

1. Barnett R. Alzheimer's disease. Lancet 2019;393:1589.
2. Patterson C. World Alzheimer Report 2018—the state of the art of dementia research: new frontiers. London: Alzheimer's Disease International (ADI); 2018: 1–48.
3. Citron M. Alzheimer's disease: strategies for disease modification. Nat Rev Drug Discov 2010;9:387–98.
4. Viña J, Sanz-Ros J. Alzheimer's disease: only prevention makes sense. Eur J Clin Invest 2018;48:e13005.
5. Jagust W. Imaging the evolution and pathophysiology of Alzheimer disease. Nat Rev Neurosci 2018;19:687–700.
6. Hardy J, Selkoe DJ. The amyloid hypothesis of Alzheimer's disease: progress and problems on the road to therapeutics. Science 2002;297: 353–6.
7. Nalivaeva NN, Turner AJ. Targeting amyloid clearance in Alzheimer's disease as a therapeutic strategy. Br J Pharmacol 2019;176:3447–63.
8. Wang YJ. Alzheimer disease: lessons from immunotherapy for Alzheimer disease. Nat Rev Neurol 2014;10:188–9.
9. Cavalli A, Bolognesi ML, Minarini A, et al. Multi-target-directed ligands to combat neurodegenerative diseases. J Med Chem 2008;51:347–72.
10. Zhang P, Xu S, Zhu Z, Xu J. Multi-target design strategies for the improved treatment of Alzheimer's disease. Eur J Med Chem 2019;176:228–47.
11. de Freitas Silva M, Dias KST, Gontijo VS Jr., et al. Multi-target directed drugs as a modern approach for drug design towards Alzheimer's disease: an update. Curr Med Chem 2018;25:3491–525.
12. Lee S, Zheng X, Krishnamoorthy J, Savelieff MG, et al. Rational design of a structural framework with potential use to develop chemical reagents that target and modulate multiple facets of Alzheimer's disease. J Am Chem Soc 2014;136: 299–310.
13. Li Q, He S, Chen Y, et al. Donepezil-based multi-functional cholinesterase inhibitors for treatment of Alzheimer's disease. Eur J Med Chem 2018;158:463–77.
14. Unzeta M, Esteban G, Bolea I, et al. Multi-target directed donepezil-like ligands for Alzheimer's disease. Front Neurosci 2016;10:205.
15. Anand A, Patience AA, Sharma N, Khurana N. The present and future of pharmacotherapy of Alzheimer's disease: a comprehensive review. Eur J Pharmacol 2017;815:364–75.
16. Cheignon C, Tomas M, Bonnefont-Rousselot D, et al. Oxidative stress and the amyloid beta peptide in Alzheimer's disease. Redox Biol 2018;14:450–64.
17. Doraiswamy PM, Finefrock AE. Metals in our minds: therapeutic implications for neurodegenerative disorders. Lancet Neurol 2004;3:431–4.
18. Dixon SJ, Stockwell BR. The role of iron and reactive oxygen species in cell death. Nat Chem Biol 2014;10:9–17.
19. Schedin-Weiss S, Inoue M, Hromadkova L, et al. Monoamine oxidase B is elevated in Alzheimer disease neurons, is associated with γ-secretase and regulates neuronal amyloid β-peptide levels. Alzheimers Res Ther 2017;9:57.
20. Youdim MBH. Monoamine oxidase inhibitors, and iron chelators in depressive illness and neurodegenerative diseases. J Neural Transm 2018;125:1719–33.
21. Zhuang C, Zhang W, Sheng C, et al. Chalcone: a privileged structure in medicinal chemistry. Chem Rev 2017;117: 7762–810.
22. Zhang X, Rakesh KP, Bukhari SNA, et al. Multi-targetable chalcone analogs to treat deadly Alzheimer's disease: current view and upcoming advice. Bioorg Chem 2018;80: 86–93.
23. Sang Z, Wang K, Zhang P, et al. Design, synthesis, *in-silico* and biological evaluation of novel chalcone derivatives as multi-function agents for the treatment of Alzheimer's disease. Eur J Med Chem 2019;180:238–52.
24. Bai P, Wang K, Zhang P, et al. Development of chalcone-O-alkylamine derivatives as multifunctional agents against Alzheimer's disease. Eur J Med Chem 2019;183:111737.
25. Sang Z, Song Q, Cao Z, et al. Design, synthesis and evaluation of novel dimethylamino chalcone-O-alkylamines derivatives as potential multifunctional agents against Alzheimer's disease. Eur J Med Chem 2021;216:113310.
26. Lee GY, Han SN. The role of vitamin E in immunity. Nutrients 2018;10:1614.
27. Qiang X, Sang Z, Yuan W, et al. Design, synthesis and evaluation of genistein-O-alkylbenzylamines as potential multifunctional agents for the treatment of Alzheimer's disease. Eur J Med Chem 2014;76:314–31.
28. Sang Z, Qiang X, Li Y, et al. Design, synthesis and evaluation of scutellarein-O-alkylamines as multifunctional agents for the treatment of Alzheimer's disease. Eur J Med Chem 2015; 94:348–66.
29. Sang Z, Wang K, Shi J, et al. The development of advanced structural framework as multi-target-directed ligands for the treatment of Alzheimer's disease. Eur J Med Chem 2020;192: 112180.
30. Sang Z, Wang K, Shi J, et al. Apigenin-rivastigmine hybrids as multi-target-directed ligands for the treatment of Alzheimer's disease. Eur J Med Chem 2020;187:111958.
31. Wang LL, Du Y, Li SM, et al. Design, synthesis and evaluation of tetrahydrocarbazole derivatives as potential hypoglycemic agents. Bioorg Chem 2021;115:105172.
32. Sharma P, Tripathi A, Tripathi PN, et al. Design and development of multitarget-directed N-benzylpiperidine analogs as potential candidates for the treatment of Alzheimer's disease. Eur J Med Chem 2019;167:510–24.

33. Tripathi A, Choubey PK, Sharma P, et al. Design and development of molecular hybrids of 2-pyridylpiperazine and 5-phenyl-1,3,4-oxadiazoles as potential multifunctional agents to treat Alzheimer's disease. Eur J Med Chem 2019;183:111707.

34. Tripathi PN, Srivastava P, Sharma P, et al. Biphenyl-3-oxo-1,2,4-triazine linked piperazine derivatives as potential cholinesterase inhibitors with anti-oxidant property to improve the learning and memory. Bioorg Chem 2019;85:82–96.

35. Di L, Kerns EH, Fan K, et al. High throughput artificial membrane permeability assay for blood-brain barrier. Eur J Med Chem 2003;38:223–32.

36. Sang Z, Wang K, Bai P, et al. Design, synthesis and biological evaluation of novel O-carbamoyl ferulamide derivatives as multi-target-directed ligands for the treatment of Alzheimer's disease. Eur J Med Chem 2020;194:112265.